BRH/DEP 70-16

PB192748

NEAR FIELD INSTRUMENTATION

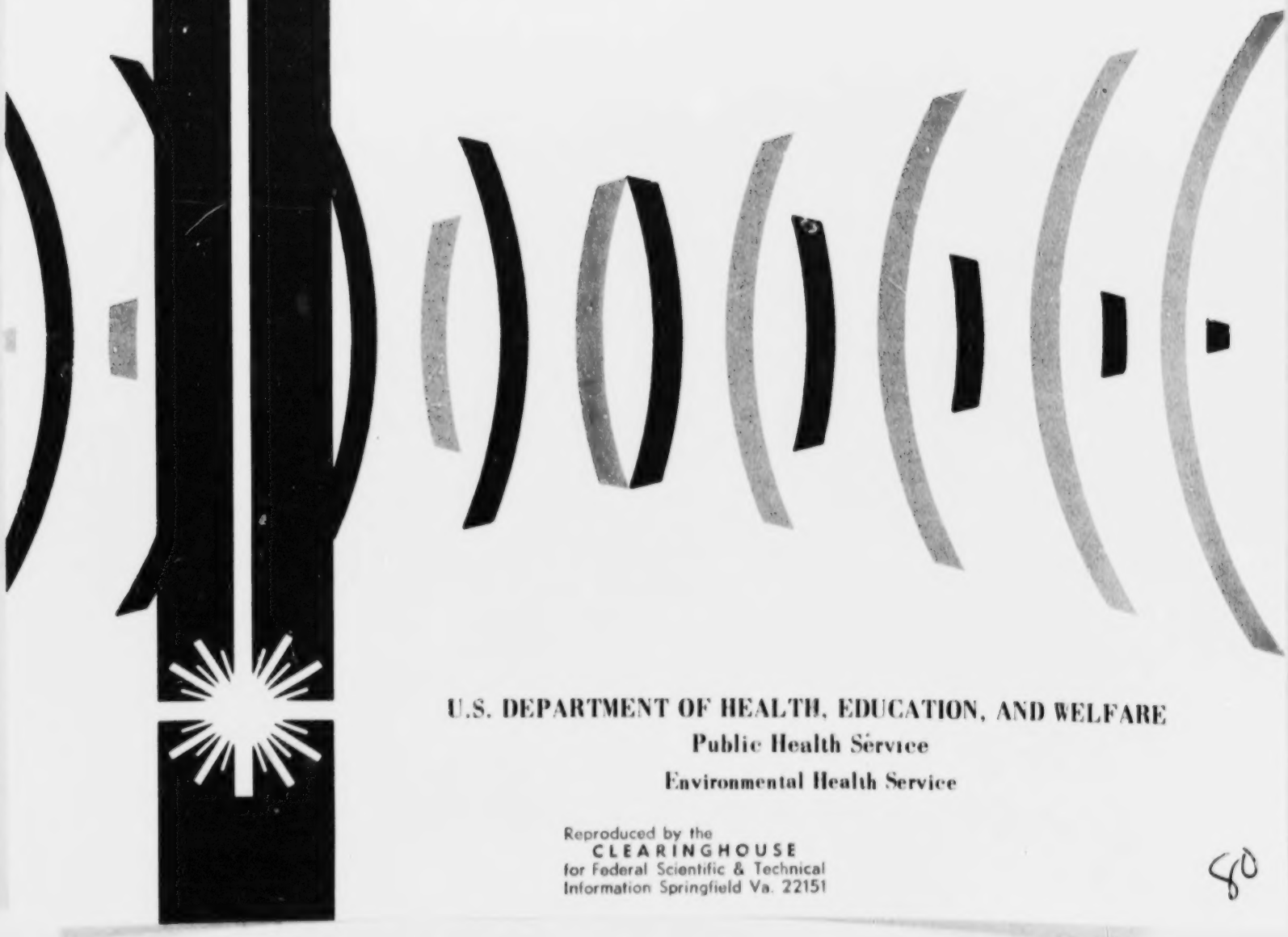

U.S. DEPARTMENT OF HEALTH, EDUCATION, AND WELFARE
Public Health Service
Environmental Health Service

Reproduced by the
CLEARINGHOUSE
for Federal Scientific & Technical
Information Springfield Va. 22151

80

DIVISION OF ELECTRONIC PRODUCTS

List of Publications

The following reports published as part of this series by the Division of Electronic Products, Bureau of Radiological Health, are available from the Clearinghouse for Federal Scientific and Technical Information, Springfield, Virginia 22151. Price is $3.00 for paper copy and $0.65 for microfiche. The PB number, if indicated for a report, should be cited when ordering.

	Title	
TSB-1	Instrument for Measurement of X-ray Emission from Television Sets (January 1968)	PB 178 808
TSB-2	A Pilot Survey of X-radiation Emissions from Color Television Receivers (In Pinellas County, Florida) (June 1968)	PB 178 809
TSB-3	A Survey of X-radiation from Color Television Sets in the Washington, D.C. Metropolitan Area (March 1968)	PB 178 810
TSB-68-4	Biological Aspects of Microwave Radiation - A Review of Hazards (July 1968) (Reprinted August 1969)	PB 185 964
TSB-5	Report of Preliminary Measurements of Electromagnetic Radiation Fields Near Microwave Ovens (December 1968)	PB 185 967
DEP 69-1	X-radiation Control Programs in the Color Television Industry - Summary Report on Visits to Manufacturers - May 1968-December 1968 (March 1969)	PB 185 979
DEP 69-2	A Field Method for the Determination of Lead in Glass Used for Shielding Television Receiver Components (December 1969)	PB 188 703
BRH/DEP 70-1	X-ray Emission from Cold-Cathode Gas Discharge Tubes Used for Educational Purposes (February 1970)	PB 189 890
BRH/DEP 70-2	Report of Tests Made on the Westinghouse Panoramix^{R} X-ray Machine (March 1970)	PB 190 870
BRH/DEP 70-3	Description and Evaluation of a Fluoroscopic Screen Visual Brightness Comparer (March 1970)	PB 190 399

(continued on inside of back cover)

BRH/DEP 70-16

NEAR FIELD INSTRUMENTATION

Prepared by

A.W. Rudge and R.M. Knox

IIT Research Institute
Technology Center
Chicago, Illinois 60616

under

Public Health Service Contract CPE-R-69-23

for

Radiation Measurements and Calibration Branch
Division of Electronic Products

July 1970

U.S. DEPARTMENT OF HEALTH, EDUCATION, AND WELFARE
Public Health Service
Environmental Health Service
Bureau of Radiological Health
Rockville, Maryland 20852

The mention of commercial products, their source, or their use in connection with material reported herein is not to be construed as either an actual or implied endorsement of such products by the Department of Health, Education, and Welfare, Public Health Service.

This report was prepared pursuant to a Government sponsored contract. The conclusions are those of the authors. Neither the United States nor the Department of Health, Education, and Welfare nor any agency or person acting on behalf of the Department of Health, Education, and Welfare makes any warranty or representation, express or implied, with respect to the accuracy, completeness, or usefulness of the information contained in this report.

FOREWORD

The Bureau of Radiological Health, formerly the National Center for Radiological Health, continues to carry out a national program designed to reduce the exposure of man to hazardous ionizing and nonionizing radiation.

Within the Bureau, the Division of Electronic Products (1) develops and administers performance standards for radiation emissions from electronic products, (2) studies and evaluates emissions of and conditions of exposure to electronic product radiation and intense magnetic fields, (3) conducts or supports research, training, development, and inspections to control and minimize such hazards, and (4) tests and evaluates the effectiveness of procedures and techniques for minimizing such exposures.

The Bureau publishes its findings in Radiological Health Data and Reports (a monthly publication), Public Health Service numbered reports, appropriate scientific journals, and technical report series for the Bureau's divisions, offices, and laboratories.

The technical reports of the Division of Electronic Products (DEP) allow comprehensive and rapid publishing of the results of intramural and contractor projects. The reports are distributed to State and local radiological health program personnel, Bureau technical staff, Bureau advisory committee members, university radiation safety officers, libraries and information services, industry, hospitals, laboratories, schools, the press, and other interested individuals. These reports are also included in the collections of the Library of Congress and the Clearinghouse for Federal Scientific and Technical Information.

I encourage the readers of these reports to inform the Bureau of any omissions or errors. Your additional comments or requests for further information are also solicited.

John C. Villforth
Director
Bureau of Radiological Health

PREFACE

This report presents the results of work performed by IIT Research Institute under contract with the Division of Electronic Products, Bureau of Radiological Health, during the six-month period from July 1969 to December 1969. The project was initiated because of the difficulty that was being encountered in measuring electromagnetic radiation leakage from microwave ovens and the need for improved measurement instruments. This report defines many of the problems associated with the measurement of electromagnetic radiation, discusses possible solutions, and describes the near-field probe which was developed during the project.

The work described herein was accomplished by Dr. A. W. Rudge and Mr. R. M. Knox of IIT Research Institute. Their diligence and sincerity of effort in the performance of this contract is appreciated.

Robert L. Elder, Sc.D.
Acting Director
Division of Electronic Products

CONTENTS

		Page
FOREWARD		iii
PREFACE		v
FIGURES		viii
ABSTRACT		ix
I.	INTRODUCTION	1
II.	FAR-FIELD CALIBRATION	3
III.	NEAR-FIELD MEASUREMENTS - SOURCES OF CALIBRATION ERROR	6
IV.	BASIC PROBE CONFIGURATION	10
V.	POWER DETECTION METHODS	12
VI.	DYNAMIC RANGE AND SENSITIVITY	16
VII.	SCATTERING	22
VIII.	FIELD CURVATURE	39
IX.	POWER DENSITY CALIBRATION	44
X.	PROBE POLARIZATION	55
XI.	FINAL FORM OF THE PROTOTYPE PROBE	58
XII.	CONCLUSIONS AND SUGGESTIONS FOR FURTHER WORK	65
REFERENCES		69

FIGURES

		Page
1.	The basic probe configuration	2
2.	The coaxitube dipole	17
3.	Dynamic range characteristic of basic probe configuration with load resistance switched at 10 mV output	19
4.	Showing variation of output voltage with wing length for basic probe configuration. Probe immersed in field strength of 5 volts/meter field strength at 2450 MHz	21
5.	The slotted groundplane test site	23
6.	The reflectometer block schematic	25
7.	Slot field power distribution and reflected power distribution. Probe scanned at 2 cm above groundplane along slot axis. Peak reflected power = 10 percent of total power transmitted	27
8.	Relative reflected power when probes with wing lengths given are passed along slot at 2 cm above groundplane	28
9.	Relative reflected power for diode probe scanned 2 cm over slot with diode reverse bias shown	29
10.	Variation of resonant dipole impedance with height (r) above slotted groundplane. (i) resistance (ii) reactance f = 2450 MHz	31
11.	Variation in dipole impedance above a large groundplane for resonant and short dipoles. (i) resistance (ii) reactance f = 2450 MHz	33
12.	Illustrating effect of dipole impedance variation on field strength measurements. Field strength measurements approaching a 6.1 cm slot in a large groundplane	35
13.	(a) The nomenclature for the "effective height" (h_e) calculation	40
	(b) The variation of $(h_e)^2$ as the probe approaches the slot	41
14.	Coordinate system for the case of a slot in an infinite groundplane	46
15.	Ratio of $(W_2)/(W_1)$	49
16.	Experimental data supporting the potential error curves of figure 15	51
17.	With electric field probe approaching a single current element (T.M.source)	53
18.	Ratio of $(W_2'')/(W_1')$	54
19.	The crossed dipole-diode configuration	56
20.	The prototype probe	59
21.	The prototype probe dynamic range measurements	62

ABSTRACT

A near-field probe for measuring electromagnetic radiation was developed. The probe employs diode detectors and is designed to minimize interactions with the field being measured. This report discusses the problems associated with measuring electromagnetic radiation and describes the design, construction, and calibration of the prototype probe.

NEAR FIELD INSTRUMENTATION

I. INTRODUCTION

The objective of this report is to describe an experimental study leading to the design, construction and calibration of a prototype near-field electromagnetic radiation probe, with an output calibrated in terms of power density. Before such a probe can be designed it is necessary to consider the problems involved in making accurate near-field measurements, particularly when the output indication is required to be as specified above. The general approach followed here has been the use of an electric field strength probe with an output calibrated in terms of power density. For reasons given in the following sections the field sensing device selected was a silicon point contact diode, and the probe antenna type that of a small dipole. The general probe configuration evaluated is shown in Fig. 1. The terminology employed with reference to the probe is also indicated in this figure.

Before considering the problems associated with near-field measurements it is in order to briefly review the derivation of the free space (or far-field) power density calibration factor applicable to the probe. This factor converts a measurement of electric field strength to a power density indication when the probe is immersed in a uniform linearly polarized, electric field, radiated from a distant source. A source time function of form $e^{j\omega t}$ is assumed where "ω" is the radian frequency and "t" is in seconds.

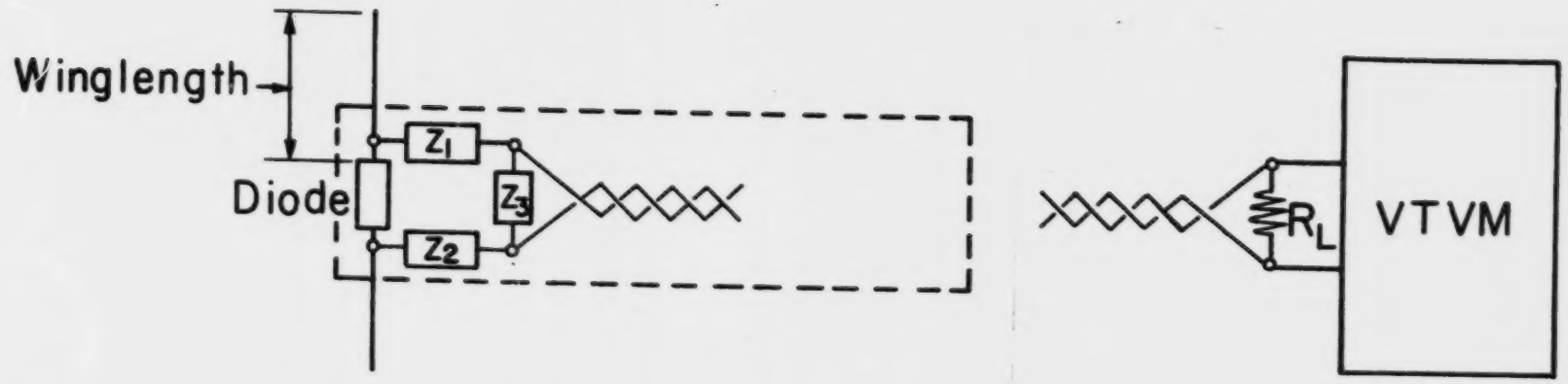

Figure 1. The basic probe configuration.

II. FAR-FIELD CALIBRATION

An electric field probe is normally calibrated by immersing the probe antenna in a uniform, normally incident, linearly polarized field of known strength. In the case of a dipole antenna the rms open circuit voltage (V) induced in the antenna is related to the magnitude of the incident field (E) by a factor termed the "effective height" (h_e) of the antenna, such that $\sqrt{2}\ V = h_e |E|$. With a load impedance (Z_L) terminating the dipole wings the rms voltage across the load (V_L) is given by[1,2,3]

$$V_L = \frac{h_e |E|\ Z_L}{\sqrt{2}\ (Z_a + Z_L)} \qquad (1)$$

where Z_a is the total impedance of the antenna, including dissipation losses and any reactance arising from the termination of the antenna at the feed point.

With a time dependence of the form $e^{j\omega t}$ the average power per unit area of such a field, over a cycle of the source frequency, can be expressed using Poyntings vector as[1]

$$\vec{P} = \frac{1}{2} R_e(\vec{E} \times \vec{H}^*) \qquad (2)$$

where $\vec{E}$ and $\vec{H}$ represent the time varying electric and magnetic field vectors, with magnitudes $|E|$ and $|H|$ respectively and * denotes the complex conjugate. Only mutually orthogonal components of $\vec{E}$ and $\vec{H}$ contribute to the power flow and the direction of the flow is normal to the plane containing $\vec{E}$ and $\vec{H}$.

In a free space environment far from the source, a linearly polarized field has one spatially orthogonal pair of electromagnetic components in time phase such that the ratio $E/H = Z_o$, where Z_o is the intrinsic impedance of free space. The average power density incident upon a probe antenna immersed in this field then becomes

$$P_i = \frac{|E|^2}{2Z_o}. \tag{3}$$

The average power absorbed in the dipole load (P_a) can be determined from Eq. (1) and is usually written,

$$P_a = \frac{h_e^2 |E|^2 R_L}{2(Z_a+Z_L)^2} \tag{4}$$

where R_L is the resistive component of the series equivalent load impedance. The calibration factor of the antenna is termed "effective aperture" (A_e) and is given by the ratio of the power absorbed in the load to that power density incident upon the dipole.

$$A_e = \frac{P_a}{P_i} = \frac{h_e^2 Z_o R_L}{(Z_a+Z_L)^2} \tag{5}$$

The "effective height" of the dipole can be expressed as

$$h_e = -\int_{-h}^{h} i(x)\, e(x)\, dx \tag{6}$$

where "i" is the current distribution along the dipole, oriented along the "x" axis, normalized to its value

at the input terminals, "e" is the component of the electric field tangential to the surface of the dipole normalized to its value at the center of the dipole, and "h" is the physical half length of the dipole.

For a uniform incident electric field Eq. (6) becomes,

$$h_e = - \int_{-h}^{h} i(x)\, dx \qquad (7)$$

giving approximate values of h_e of λ/π for thin half-wave dipoles (i.e., $2h = \lambda/2$) and a value of "h" for thin dipoles with $2h << \lambda$.

A useful additional relationship, valid in the free space environment, relates the "effective aperture" of an antennna with its overall power gain

$$A_e = \frac{\lambda^2}{4\pi} G. \qquad (8)$$

where G is the overall antenna gain relative to an isotropic reference. Knowledge of the probe antenna gain by comparison with a standard gain antenna thus provides the effective aperture calibration factor directly.

III. NEAR-FIELD MEASUREMENTS - SOURCES OF CALIBRATION ERROR

The sources of a potential error in making near-field measurements will be considered in two main steps. The errors which may be incurred in making a measurement of the electric field strength close to an electromagnetic source and the additional problems involved in attempting to convert this measurement of electric field strength into an indication of power density by means of a calibration factor.

When a probing antenna is immersed in an electromagnetic field some level of perturbation of the field is unavoidable. The perturbation arises in part from the non-transparency of the probe body and feed to the incident field, but principly due to re-radiation from the probe antenna. A certain part of the re-radiation from the antenna is a necessary function of its operation and provides the mechanism by means of which some of the incident power is absorbed in the antenna load.[4] The total back-scatter arising from a dipole antenna is spatially distributed over a large solid angle and its magnitude relative to the incident power density is a function of the antenna and load parameters.[3,5] In free space measurements antenna back-scatter tends to be unimportant in that the ratio of the incident field strength to the voltage developed across the antenna load remains a constant.

In a near-field measurement, however, back-scatter from the probing antenna may be of sufficient magnitude to significantly modify the source field and thus bring about a change in the resultant field incident upon the probe. Under these conditions 'multiple coupling' is said to occur between probe and source, thereby invalidating the measurement. In many practical near-field measurements the electromagnetic source is associated with a large metallic geometry and back-scatter from the probe may be reflected back to the probe antenna. Under these circumstances the reflected

field may be considered to modify the impedance of the probing antenna with a subsequent effect on the electric field calibration (i.e., see Eq. (1)).

The electric field incident upon a probe antenna located at a large distance from an electromagnetic source can be considered to have a plane wavefront. In the near-field, however, the wavefront may exhibit considerable curvature. Under conditions of field curvature the approximation implied in Eq. (7) is no longer valid and the "effective height" parameter must be determined from Eq. (6), thus requiring a knowledge of both the probe antenna current distribution and the spatial distribution of the electric field under measurement.

To achieve accurate measurements of electric field strength close to a source the problems associated with field curvature and back-scatter, particularly with regard to multiple coupling and impedance variation, present the major difficulties. The extent of these problems will be examined in the following sections. The conversion of such field strength measurements to power density indications, however, raises further complications.

In the region close to a periodically time varying electromagnetic source the Poynting vector will be complex and can be considered to indicate both real power flow and the reactive power flow present in the vicinity of the source. The average power flow per unit area over a cycle of the source frequency will still be given by Eq. (2) but the modal structure in this region may not be purely transverse (TEM) as in the far-field case. Hence, the approximation that $E/H = Z_o$ implied in Eq. (3) is not necessarily valid, and the power density indicated by the probe calibration may differ from the true density indicated by Eq. (2).

An additional power calibration error exists for electric field probes when the mode existing at the source is transverse magnetic (TM). In this case, there may be an electric field component which is associated with a purely reactive power. The average power density of this reactive power as given by Eq. (2) will be zero, however, the probe antenna will respond to the electric field component and indicate a real power density.

The problems involved in making near-field measurements are obviously not independent of the particular source involved, and the geometry of the source structure. The approach taken here is an examination of the critical parameters involved to determine the source-probe separation at which the far-field calibration can be assumed accurate, within given limits, for practical source configurations. The configurations chosen are: the slot in a conducting ground plane, which is a predominantly TE mode source and typical of many radiation leakage situations; and the thin dipole radiator, which serves as a predominantly TM mode source. The work described here is largely confined to measurements close to TE mode sources, however, some of the additional problems associated with TM sources are briefly considered.

Worse case current distributions (magnetic for the slot, electric for the dipole) with respect to calibration error are defined to implement the study. Three basic questions require answers. At what minimum probe-source separation does the probe output with a far-field calibration cease to give a reliable indication of the electric field strength present in the absence of the probe? To what minimum separation can this measured electric field be expressed as a true power density by use of the far-field calibration factor? To what extent can this separation be minimized by suitable probe design?

Before proceeding with this study the choice of the basic form of the probe antenna employed in this work will be briefly discussed.

IV. BASIC PROBE CONFIGURATION

The basic requirements for a near-field probe are that its antenna sampling area should be small and that the introduction of the probe into the field to be measured introduces a minimal perturbation of that field. Ignoring for the present the problem of re-radiation from the probe antenna, the probe body is required to be as near transparent to the incident field as is possible.

For the probe antenna either a small thin dipole, or a tapered waveguide will provide small sampling areas. The waveguide can be loaded with a dielectric to permit its aperture dimensions to be reduced to values which would not, in the absence of the dielectric, support a propagating mode. However, the metallic walls of the waveguide tend to perturb the field under measurement and thus the dipole has advantages in this respect providing the feed system can be suitably arranged. While the dipole is a linearly polarized antenna, orthogonal configurations are possible which provide outputs independent of the polarization of the incident wave.

Detection of the signal from the antenna can be achieved by the use of diode detectors, thermistors available, both compensated and uncompensated, or thermo-couples. To ease the feed line perturbation problem it is desirable that the RF portion of the probe be confined to the immediate vicinity of the antenna, thus the detection system must be situated directly behind the antenna.

The problem of back-scatter due to probe antenna re-radiation and the presence of the feed lines is examined in more detail in Section VII while the detection systems are evaluated in Sections V and VI.

The basic form of the near-field probe is shown in Fig. 1. Z_1 and Z_2 were intially two microwave chokes although later two 1/16 watt 1 KΩ miniature resistors were substituted.

The values of the resistors were chosen empirically to be low as possible while maintaining sufficient probe sensitivity with respect to the minimum electric field to be measured. It was considered that in the event of an electromagnetic transient, such as static discharge, producing a large reverse voltage across the diode, that the lower impedance offered by the series circuit of resistance and capacitance would help to protect the diode. Z_3 is a 500 pf microwave chip capacitor to confine the RF to the diode circuit and the dc feed wires comprise two tightly twisted small diameter insulated wires The probe output is indicated on a vacuum tube voltmeter (VTVM). The diode detector selected was a silicon point contact diode type MA 41512 (see Section V).

V. POWER DETECTION METHODS

A. Introduction

All of the devices considered can be placed in one of two broad categories. First, the devices which measure microwave power through sensing a change in temperature make up one class of devices. The second type of device is that which directly produces a current or voltage due to the electromagnetic energy. In the first class of devices are included thermocouples and bolometers, while the primary example of the second type of device is the semiconductor diode.

B. Thermal Sensing Devices

1. Bolometers

Various types of bolometers (thermisters, barretters, etc.) have been developed for microwave power measurement. They operate on the principle that a resistance change with temperature in the bolometer is measured in a sensitive bridge circuit. The incident microwave energy induces a temperature change in the bolometers which thereby produces a measurable unbalance in the bridge circuit.

A primary disadvantage of bolometers, and all temperature sensing devices, is that they not only measure microwave power changes, they also measure ambient temperature changes. This causes an objectionable drift in the instrument. This drift ultimately limits the sensitivity of the instrument. A number of bridge circuits have been developed, however, in which a second thermistor element is used for temperature compensation. The second thermistor is also located at the power sensing probe. In one type of circuit, the thermistors are connected in parallel in the RF circuit but in series in the dc bridge circuit in order to achieve temperature compensation.(6)

Commercially available bolometer power meters* have been been developed which offer good sensitivity (1 microwatt) and low drift but which use rather complicated bridge circuits.

2. Thermocouples

A thermocouple can be used to measure microwave power. It merely uses a millivoltmeter to determine the power level. However, being a temperature sensitive device it also will drift with ambient temperature changes and, therefore, requires temperature compensation. Commercial microwave power meters and probes** are now becoming available which use thermocouples, but the requirement for temperature compensation necessarily complicates the associated electronic circuitry.

C. Direct Electromagnetic Sensors

A nonlinear semiconductor diode can be used to detect microwave energy. The nonlinearity is used to convert the microwave signal to a dc signal for detection. Suitable filtering of the microwave signal is provided to prevent coupling into the dc circuitry.

The diode detector has a region of "linear" detection and a region of "square-law" detection. The former occurs for input signals of approximately +5 dBm (dB referenced to one milliwatt) and larger and the latter for input signals of approximately -10 dBm and smaller. In the present application the detector is employed for direct power measurement, or as a square law detector.

For small signals the approximate current-voltage relationships of the diode is represented by the Taylor expansion[7]

$$i = f(e_o) + \frac{df}{de}(\delta e) + \frac{1}{2}\frac{d^2f}{de^2}(\delta e)^2 \qquad (9)$$

---

* Hewlett-Packard Model 431C

** Narda Model 8100

where e_o is the bias voltage at the operating point and (δe) is the input signal. The linear term, of course, is of no importance as far as signal rectification is concerned because it is symmetrical about the operating point. Thus, square law behavior is expected for signal levels small enough to assure that the above equation is valid.

The sensitivity of the diode detector is very adequate for the minimum field level specified in this program (5 V/M - about 0.007 mw/cm^2), and could be used at even lower field levels (See Section XI). A dynamic range of 40 dB is not uncommon for detector diodes used in video detectors (input power variations from -10 to -50 dBm).

Sensitivity of a typical detector diode is 400 mv/mw. This compares favorably with sensitivity values of 0.2 - 20 mv/mw for thermocouples.[8]

Since microwave power detection using a detector diode is not a thermal process, ambient temperature changes do not influence the voltage output. The influence of temperature variation on the current-voltage characteristic can affect the diode detector sensitivity but this is a second-order effect and will be negligible for normal ambient temperature changes.

D. Preferred Power Detection Devices

On the basis of the considerations discussed above with particular consideration to temperature effects, the detector diode was selected for the near-field probe. Other factors influencing this choice were: 1) diodes are inexpensive and available in conveniently small packages, 2) diodes in the proper kind of circuit have a high burnout level, and 3) associated instrumentation is of the simplest type (any sensitive high impedance dc voltmeter can be used).

Several types of diode detector were examined for suitability. The final choice was a silicon point contact diode type MA 41512.* This diode exhibited excellent sensitivity and low noise in the frequency range of interest. The diode was conveniently packaged in a small non-metallic capsule and was comparatively inexpensive. The dc reverse resistance of the diode was of the order of 10 kΩ or less which was found a usefully low impedance with regard to the reduction of pickup noise on the dc feed lines.

---

* Manufactured by Microwave Associates, Inc.

VI. DYNAMIC RANGE AND SENSITIVITY

For convenience in use it is desirable that the output voltage of the near-field probe should give an indication which is linear with respect to the incident power density over a wide dynamic range. Such an output characteristic demands that the detector diode be operated in its square law, or small signal mode. In this region the diode output current will be proportional to the square of the voltage applied via the dipole wings.

The detector diode square law characteristic exists only over a comparatively small part of the diode current/voltage (I/V) curve usually in the region of I = 0. Hence, it was necessary to determine the maximum useful range of input power (P) over which the square law relationship was valid for the silicon diode selected. With the basic probe configuration shown in Fig. 1 the output voltage developed across the microwave chip capacitor acts as a reverse bias to the diode junction. In the reverse bias direction the diode I/V characteristic rapidly departs from square law and thus it is necessary to determine the maximum value of reverse bias permissible while maintaining the square law I/V (or linear I/P) relationship. If the diode dc load resistance R_L is then decreased to prevent the reverse bias exceeding this critical value, the power input can be increased to the point where the diode departs from its square law characteristic in the forward direction.

Measurements were carried out by uniformly illuminating the basic probe from a distant microwave horn antenna. The horn was driven from a power oscillator via a precision calibrated attenuator. Absolute field strengths at the probe were measured by replacing the probe with a slot-fed dipole antenna which had been previously calibrated at 2450 MHz in an anechoic chamber. The slot fed dipole standard is shown in Fig. 2.

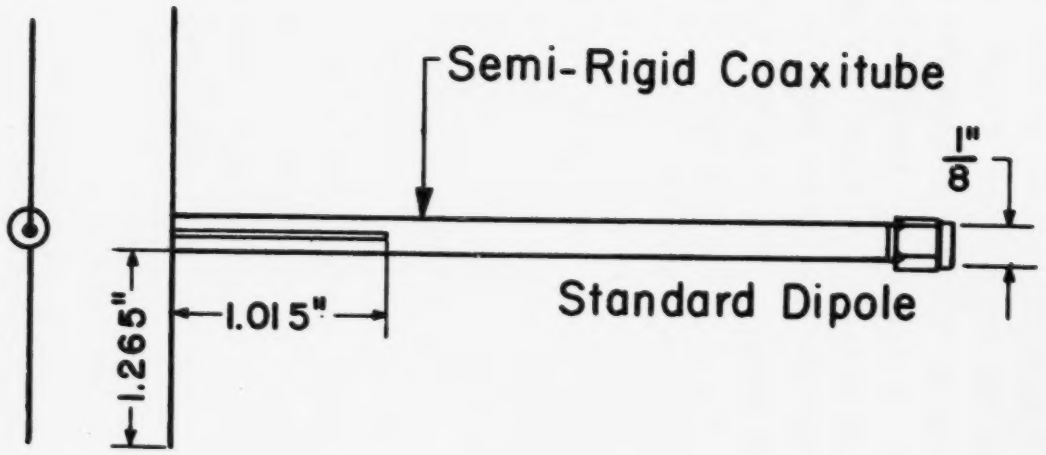

Figure 2. The coaxitube dipole.

Using a silicon diode (MA 41512) with a load of 10 KΩ on the probe dc output, changes in output voltage were found to be directly proportional to changes in input power (±0.5 dB) in the output voltage range 0 - 10 mV. With a 500 Ω dc load the change in output voltage was found to be directly proportional to input power within ±0.5 dB in the range 0 - 10 mV and within ±1.0 dB in the range 10 - 30 mV. While providing a large dynamic range the 500 Ω load seriously reduces sensitivity in that at low power levels the output voltage is extremely small. A range switch was thus incorporated to use the 10 kΩ resistance load at low power densities and the 500 Ω resistance for higher power. The scaling factor in this case is a convenient "÷ 10". Use of higher values of load resistance than 10 kΩ provided improved sensitivity but increased the tendency for pickup noise to appear on the dc feed lines. Load resistances of less than 500 Ω can be employed to further extend the square law range. The limit in this direction appeared to be when the dissipated power due to the direct current in the detector circuit feedlines and load was of the order of -13 dBm.

Figure 3 shows the probe input/output characteristics on a dB scale where 0dB output corresponds to 1 mV on the VTVM with a 10 KΩ load. The point of operation of the range switch has been indicated. The values of the probe components are also shown. It should be noted that due to manufacturing tolerances on the silicon diodes the values of dc load required may vary slightly. A practical method of selecting these values will be described later in the text (see Section XI).

If at the highest power density the direct current circuit dissipation is to be -13 dBm then with Z_1 and Z_2 (see Fig. 1) each having a value of 1 kΩ and assuming a feed line resistance of 60 ohms then the value of load resistance required to provide a 10 mV output can be calculated approximately as 63 ohms. To achieve the specified dynamic range of 40 dB then

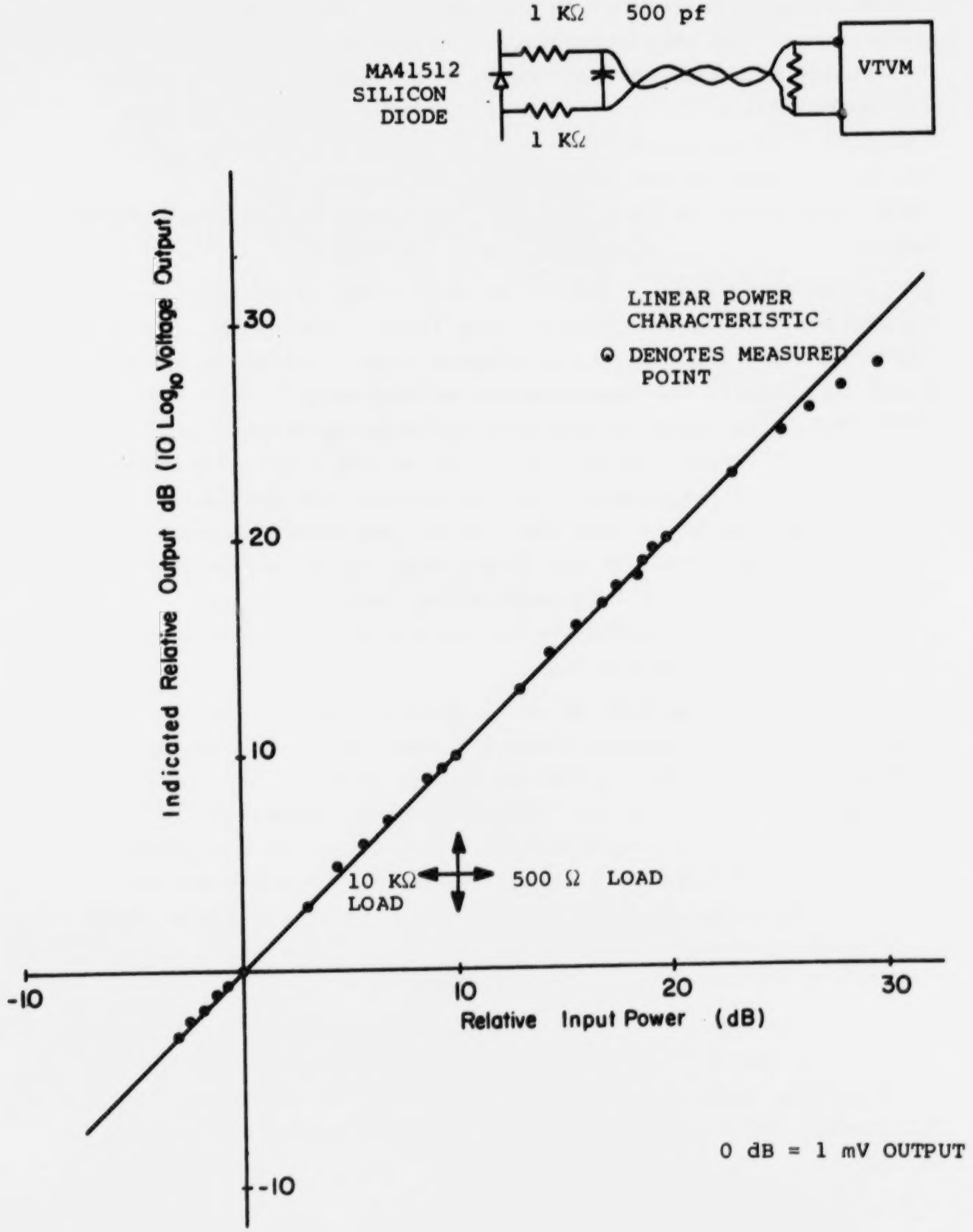

Figure 3. Dynamic range characteristic of basic probe configuration with load resistance switched at 10 mV output.

at the lowest power density the dc power dissipated in the probe circuitry will be reduced to -93 dBm as a result of the diode square law characteristics. Assuming a maximum load resistance of 10 KΩ the voltage at the probe output will then be approximately 63 μvolts. With the specified signal/noise ratio of 3 dB at the minimum power density to be measured, the noise level on the vacuum tube voltmeter (VTVM) must, therefore, be less than 32 μvolts with a 10 KΩ resistance load.

To achieve noise levels of this order it is necessary to exclude pick up from the dc feed lines. The probe used in the experimental phase of the program used extended dc feed lines to simplify the experimental arrangements. With this probe the noise level on the VTVM could be maintained at less than 20 μvolts with the aid of an additional capacitance across the load resistance (.01 microfarad) and providing that the twisted wires used for the dc path were not held directly in the hand. In its final form the prototype probe design guarded against this possibility and the dc feed lines were somewhat shorter. The additional capacitance was then omitted from the circuit.

To obtain the full 40 dB of dynamic range it is necessary that the minimum field strength of 5 volts/meter (0.0066 mW/cm^2) produce a voltage output at the VTVM of approximately 63 μvolts. The controlling parameter used to achieve this calibration was the length of the probe dipole wings (see Fig. 1). A typical measured relationship between wing length and diode output, employing the basic probe configuration of Fig. 1, is shown in Fig. 4. The high sensitivity of the diode probe is evident.

The length of the dipole wings is an important parameter in other respects. In particular the wing lengths are closely related to the back-scatter created by the probe. This aspect requires examination before the probe wing lengths can be fixed.

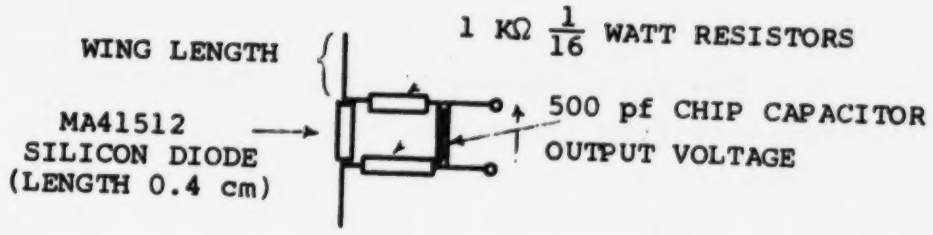

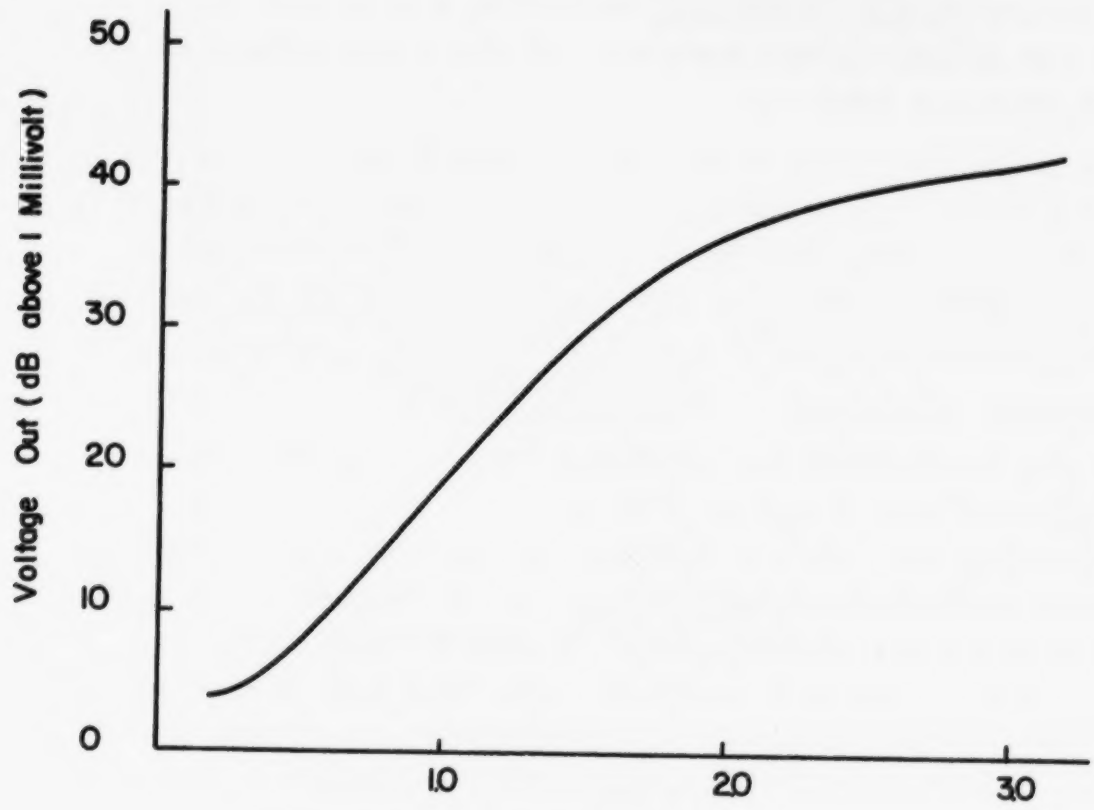

Figure 4. Showing variation of output voltage with wing length for basic probe configuration. Probe immersed in field strength of 5 volts/meter field strength at 2450 MHz.

VII. SCATTERING

The total back-scatter introduced by the basic probe originates from the probe body, the probe antenna, and the dc feed lines. In the experimental evaluation to be described, each of these sources of back-scatter is examined. The effects of back-scatter are considered from two aspects. The multiple coupling effect between probe and radiating source and the effect on the probe antenna impedance of the close proximity of a large metallic geometry.

The probe body, which was constructed from a material having a low dielectric constant ($\varepsilon_r = 1.8$) and the detector circuit components were not found to contribute significantly to the back-scatter. They are dealt with briefly in the section on "multiple coupling".

A. Multiple Coupling

In the measurement of radiation hazards the RF leakage often originates from a narrow slot or a gap in a metallic wall surrounding the source. Leakage around a microwave oven door or from a cracked waveguide might be two practical examples. Radiation from narrow slots is thus a case of particular interest in near-field measurements. For this reason an experimental site was constructed, comprised of a narrow slot in a large groundplane (see Fig. 5). The groundplane is enclosed by a wall and roof of absorbing material*. The test site was constructed for use with either dipole or monopole antennas although the monopole facility was not employed in this work. The scanning arm of the assembly is coupled to a potentiometer, thereby providing a positional input to the X axis of an XY recorder.

---

*Eccosorb CV-B9

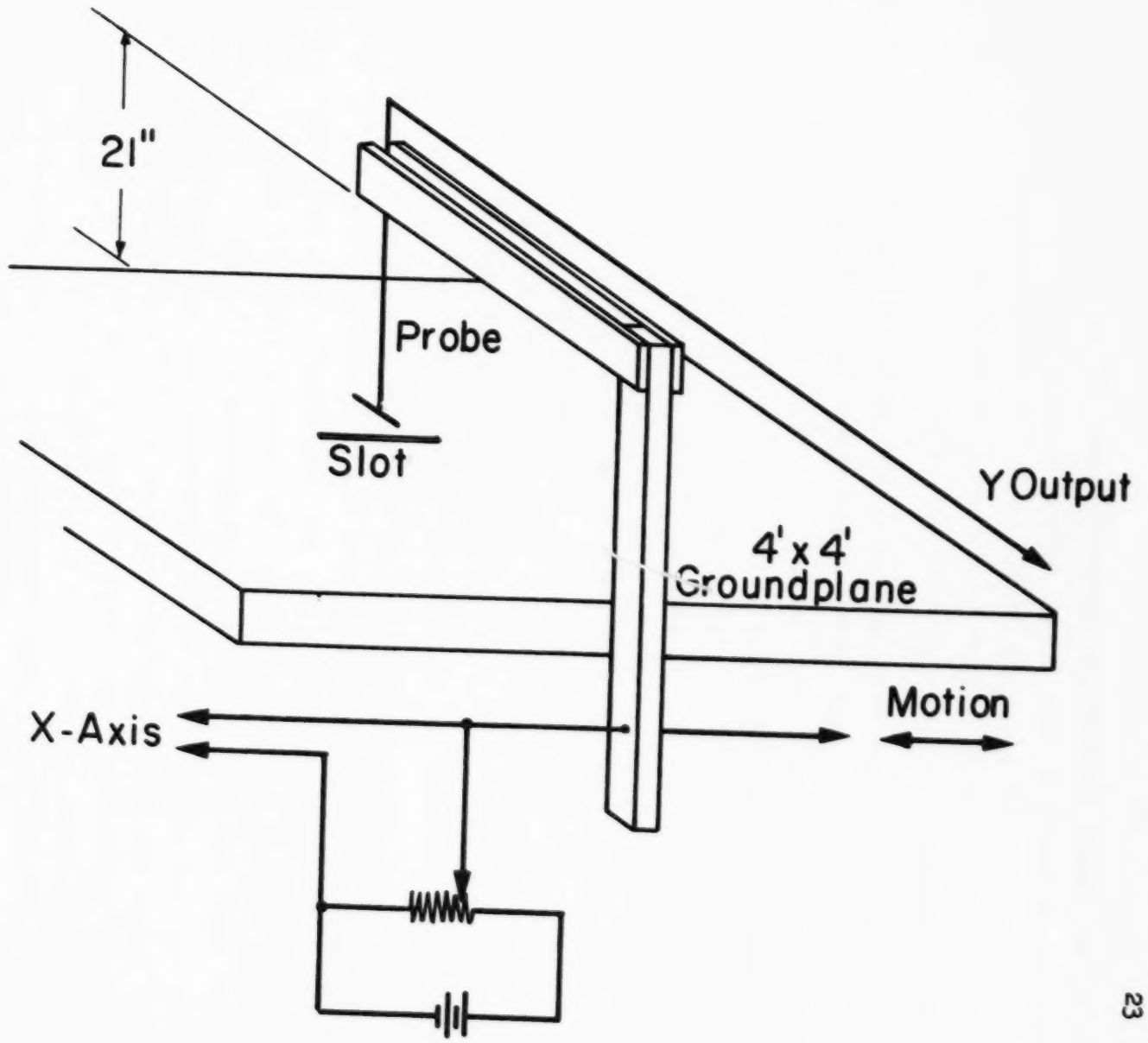

Figure 5. The slotted groundplane test site.

Using copper conducting tape to close off part of the slot and re-matching at the input to the waveguide feeding the slot by means of a triple stub tuner, the slot length was adjustable from 25 cm to 1.0 cm while still presenting a 50 Ω input impedance at the input to the slot.

At the slot input the reflectometer shown in Fig. 6 was connected to permit the measurement and display of power reflected back into the slot. Using the variable phase shifter and attenuator in the comparator loop, reflected power present prior to the introduction of the probe can be nulled. In addition, use of a precision calibrated variable attenuator in the comparator allows a measurement of the reflected power due to the presence of the probe by readjusting attenuator and phase shifter to return the null output. The change in attenuator reading will then give the power level change directly in decibels. This measurement is independent of small variations in the gain of the null detecting amplifier.

To study the possibilities of multiple coupling occuring between probe and slot, the field distribution along the slot was measured by scanning the probe along the slot axis at various slot-probe separations. The output from the probe and that from the reflectometer were plotted on the XY recorder on alternate scans. This procedure was repeated at heights above the slot ranging from 0.5 cm (0.03 λ) to 25 cm (1.5 λ) for the basic probe configuration, using wing lengths in the range 0.2 cm (0.012 λ) to 4.16 cm (0.25 λ) at a frequency of 1.806 GHz. (This frequency was chosen because of the immediate availability of components for the reflectometer.)

The probe was also scanned along the slot axis with the dipole wings cross polarized to the slot field to determine whether a significant back-scatter from the probe body and feed lines could be detected. Reflectometer measurements were also made

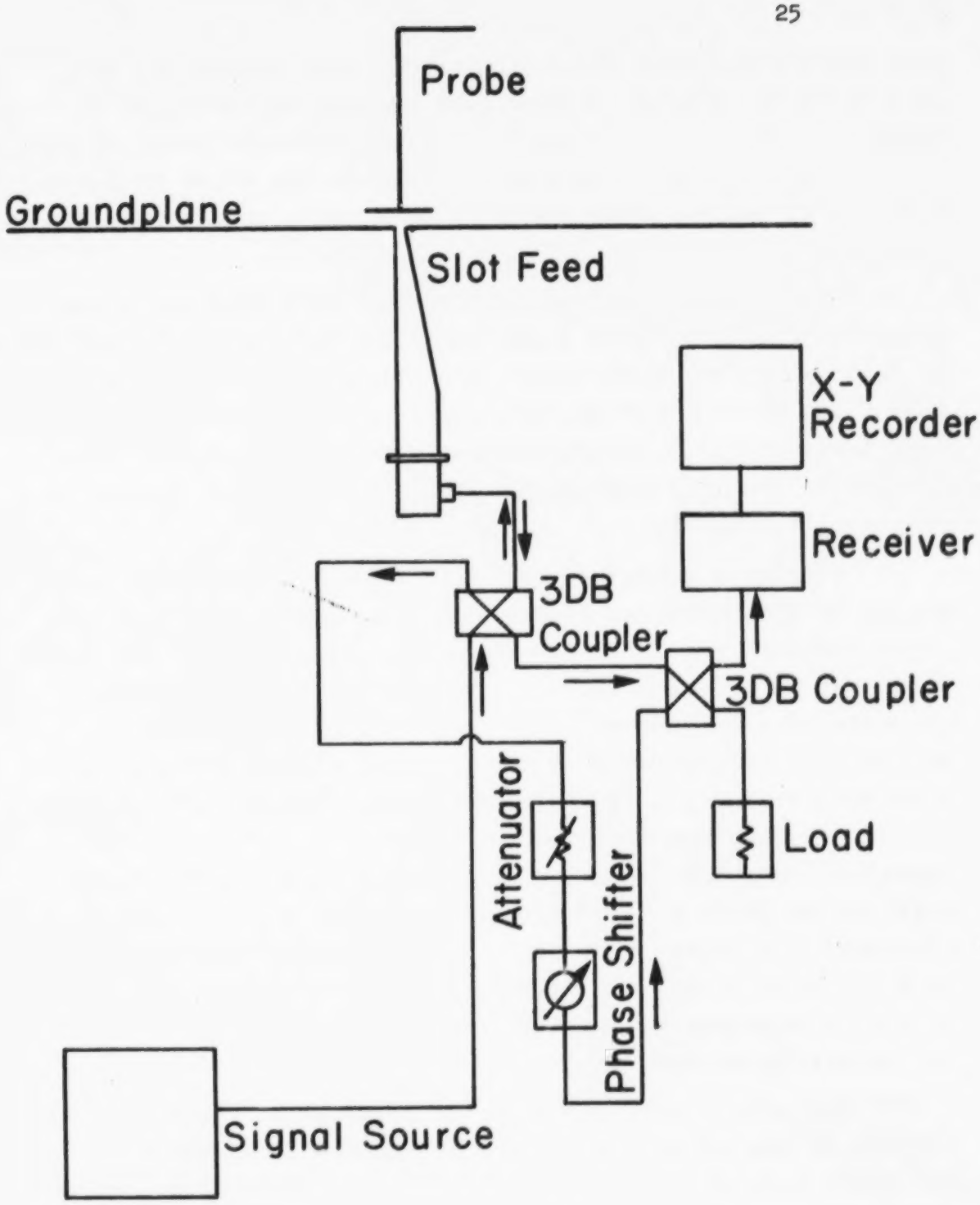

Figure 6. The reflectometer block schematic.

with the probe output short circuited, open circuited, and with different values of back bias applied to the diode to determine how critical a part the load parameter plays in the scattering process. Some typical results are shown in Figs. 7, 8, and 9. From the results certain conclusions can be drawn.

The back-scatter returned to the slot from the cross polarized probe, scanned along the slot axis, was too small to be detected at any probe-slot separation (i.e., much less than 0.01% of the transmitted power). The probe body and feed lines (in this configuration) were thus concluded to provide an insignificant contribution to the total back-scatter (see Fig. 7).

Correctly polarized the 0.25 λ wing length probe, at a height of 2 cm returned a peak reflected power of 10% of the total radiated power back to the slot. The shape of the power distribution measured by this probe at 2 cm showed little evidence of a complex multiple coupling effect, however, at the same height the very short probes, which returned an undetectable level of power to the slot, recorded essentially the same shape power distribution along the slot axis. The relative magnitudes of the distributions, using a far-field calibration in each case, differ. This was particularly noticeable at larger slot-probe spacings where multiple coupling effects are less likely. These variations are a result of the groundplane rather than the slot and will be examined in the following section.

The power level of the probe back-scatter reduces rapidly as the probe wing length is reduced (see Fig. 8). For probe wing lengths close to 0.25 λ the load on the probe wings plays a significant part in controlling the back-scatter level. A back-biassed diode or a high impedance load on the wings produces a significantly lower level of back-scatter than does a short circuit at this point. Figure 7 suggests that the

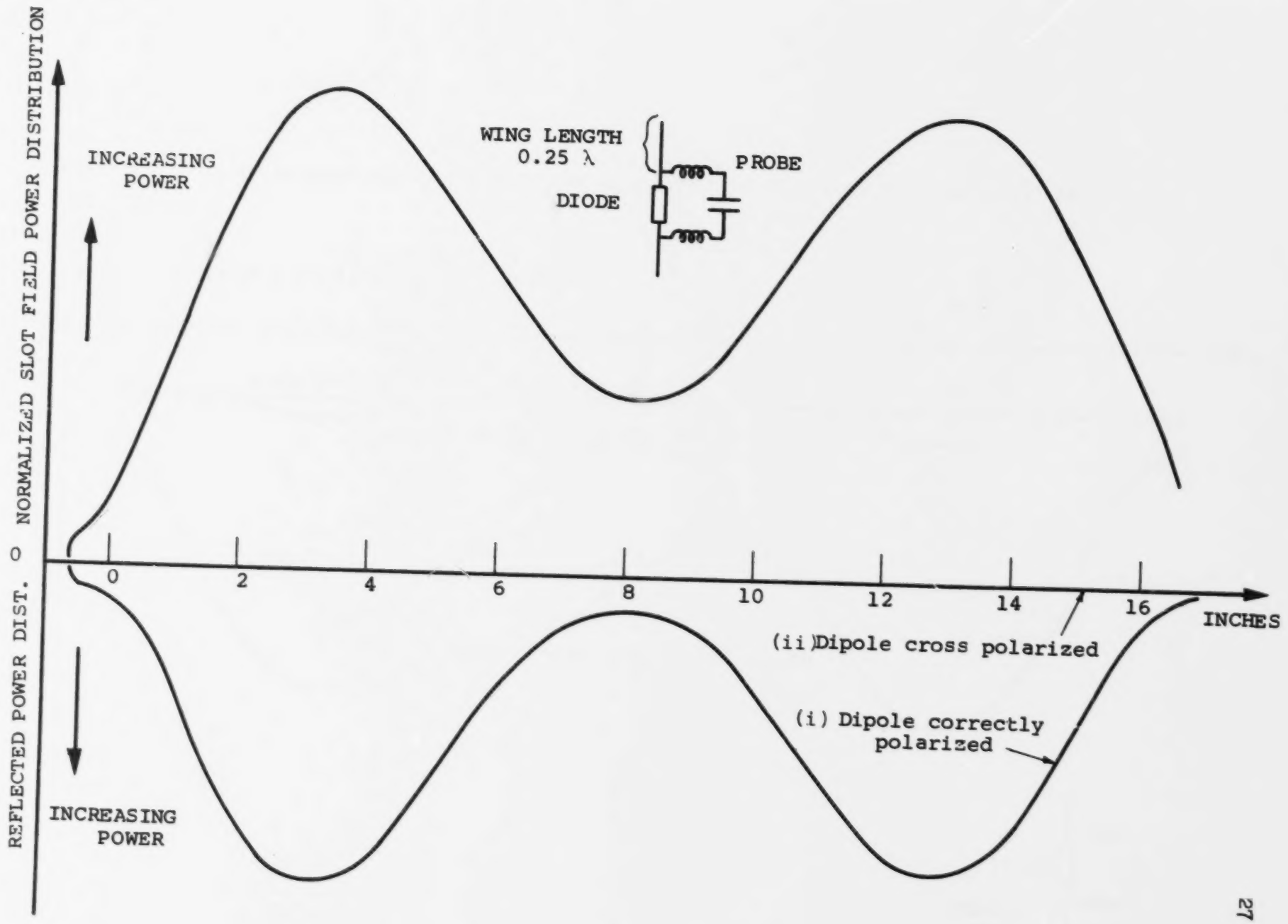

Figure 7. Slot field power distribution and reflected power distribution. Probe scanned at 2 cm above groundplane along slot axis. Peak reflected power = 10 percent of total power transmitted.

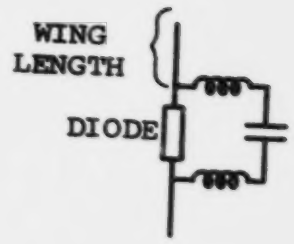

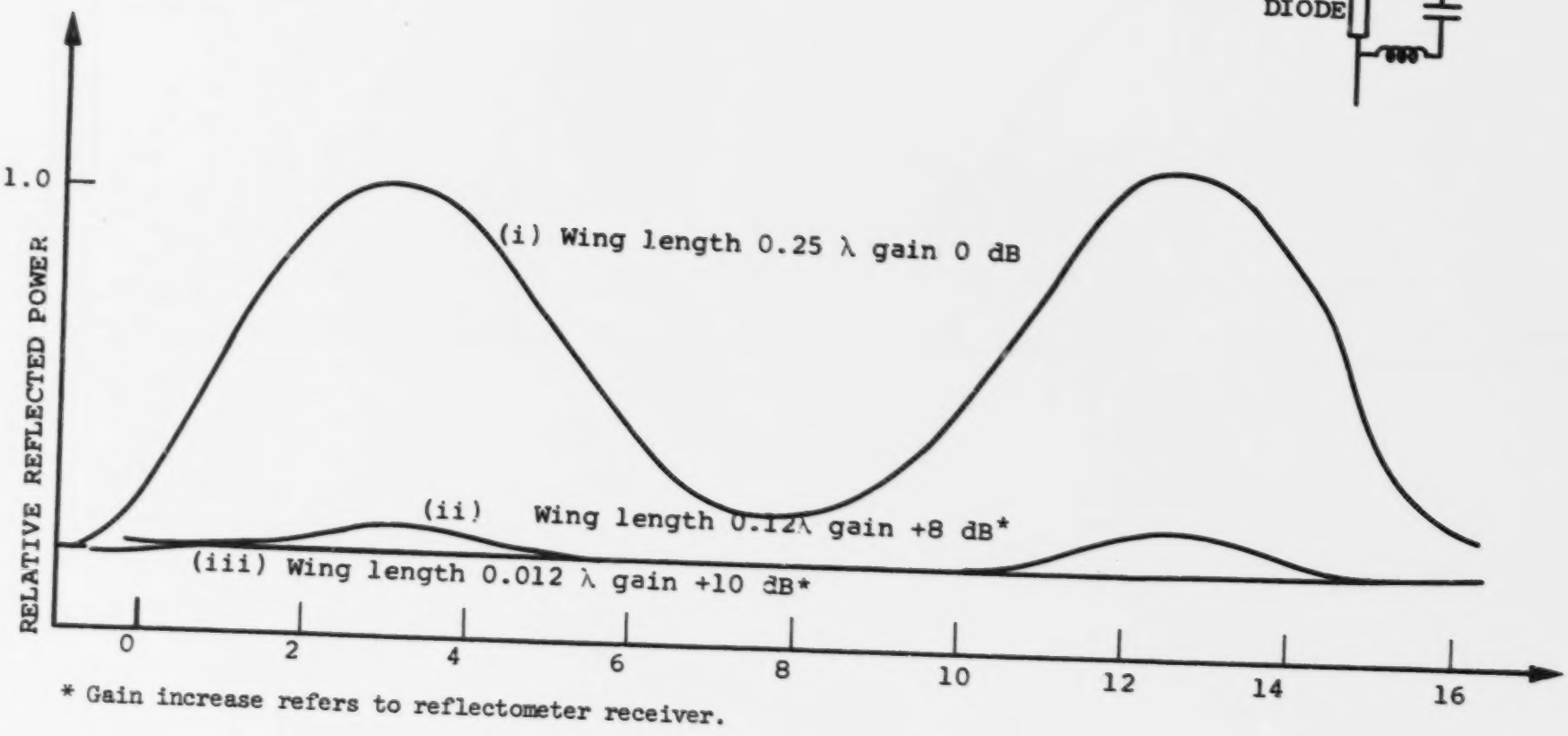

* Gain increase refers to reflectometer receiver.

Figure 8. Relative reflected power when probes with wing lengths given are passed along slot at 2 cm above groundplane.

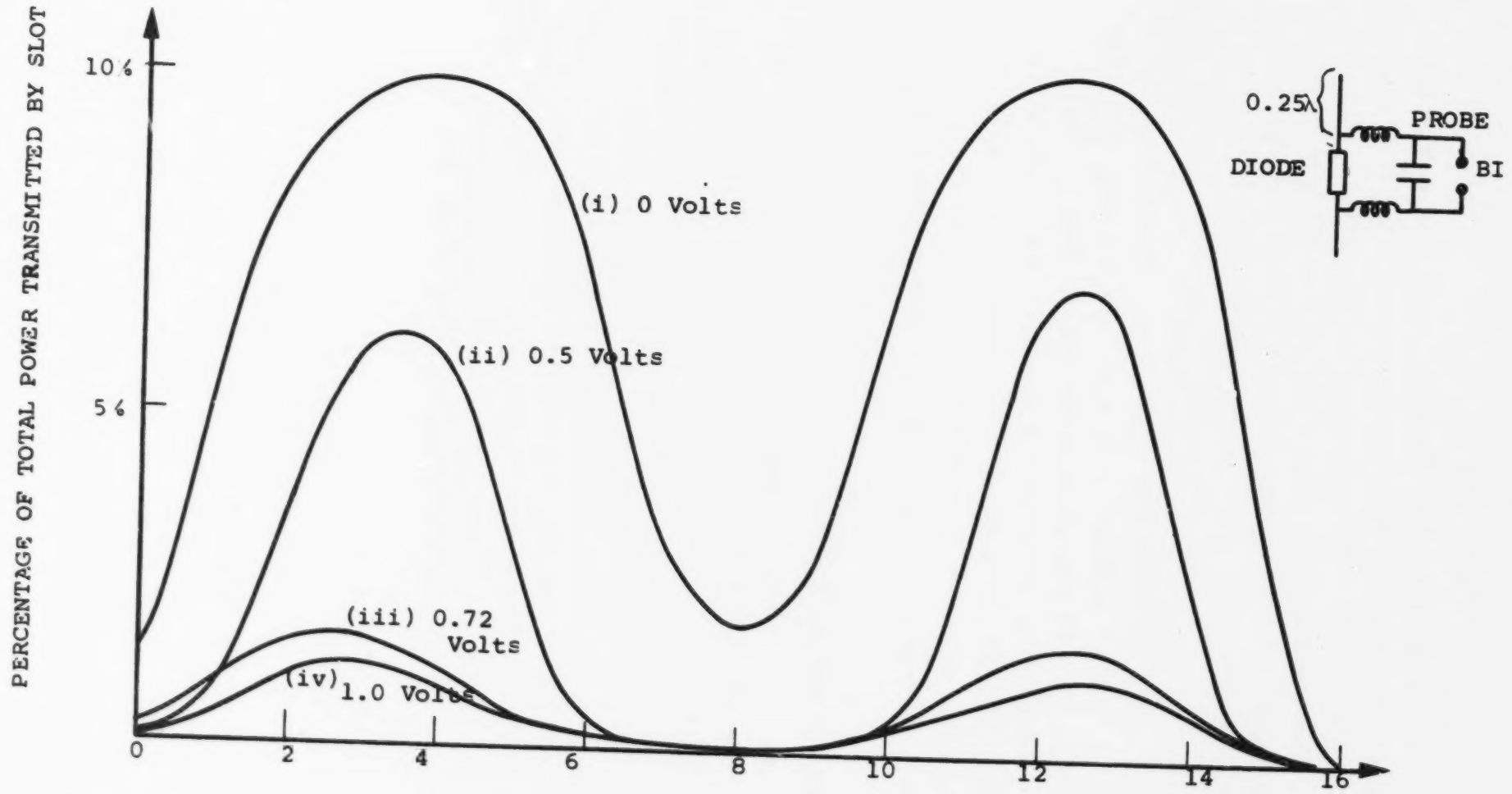

Figure 9. Relative reflected power for diode probe scanned 2 cm over slot with diode reverse bias shown.

peak power returned to the slot coincides with the peak field at the probe wings and thus with the magnitude of the current flow in the probe wings. The impedance of the dipole close to resonance is low and thus the magnitude of the current flow would be expected to be very sensitive to the RF load presented at the dipole terminals. This sensitivity is clearly illustrated in Fig. 9.

When the dipole wings are made short, however, the impedance of the wings becomes very high and the current flow excited by the incident field correspondingly small. Very little back-scatter can be detected in this case, even under short circuit load conditions and the relative importance of the load on the dipole wings is consequently diminished. Under these conditions multiple coupling effect appear to be negligible.

B. Probe Impedance Variation

When a dipole probe is situated close to a radiating slot it has been found that only a small percentage of the total radiated power is returned to the slot. However, the presence of a large metallic geometry such as the groundplane of the test site shown in Fig. 5 will result in a reflection of any incident back-scatter originating from the probe. Power reflected by this means directly to the probe can be considered to modify the probe impedance. To examine this effect, the impedance of the coaxitube dipole with 0.255 λ wings (see Fig. 2) was measured at various heights above the following:

1) a large groundplane,
2) a short (3 cm) slot in a large groundplane, and
3) a long (25 cm) slot in a large groundplane.

The measurements were carried out at 2.45 GHz by conventional slotted line techniques. The experimental results are shown in Fig. 10.

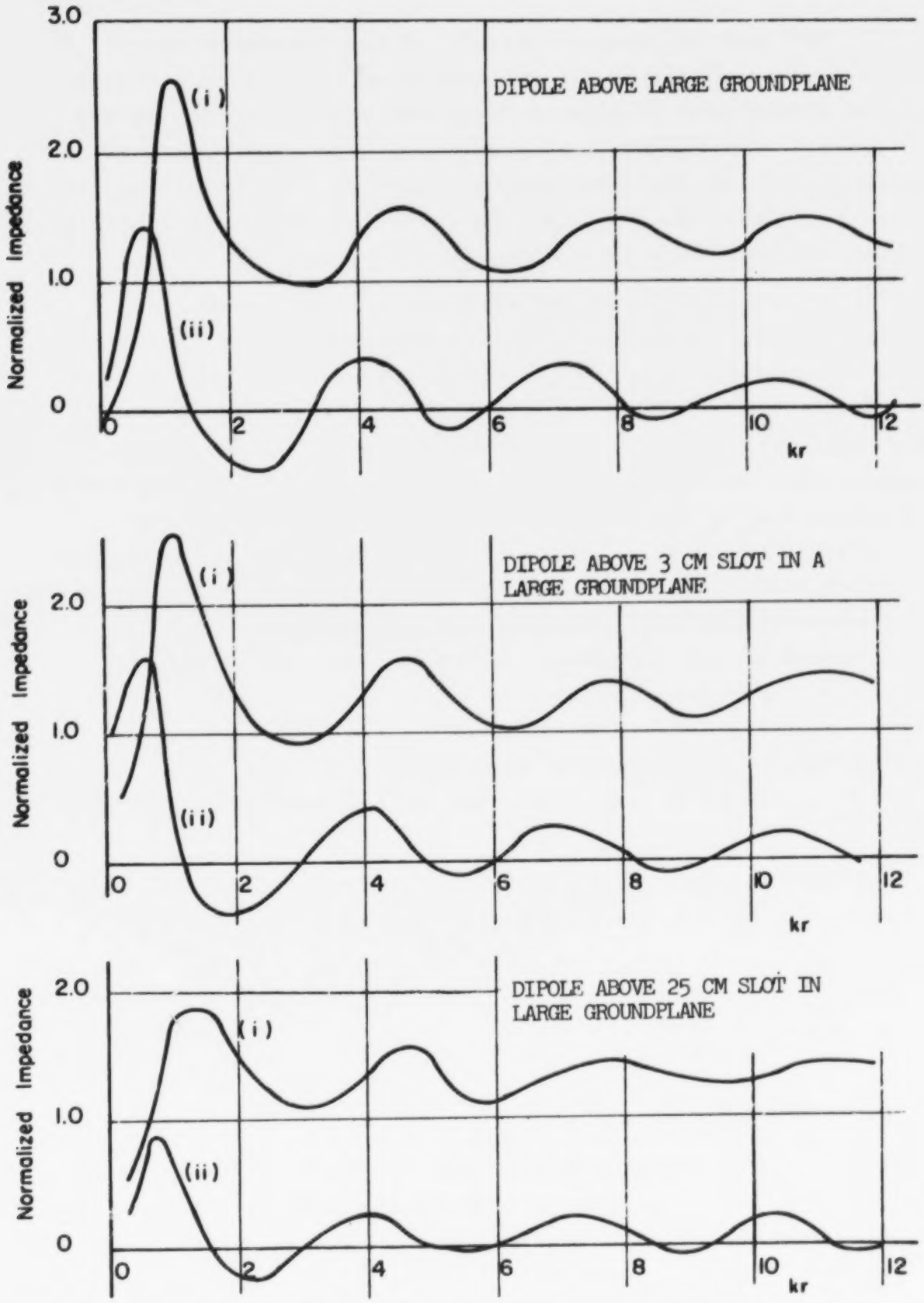

Figure 10. Variation of resonant dipole impedance with height (r) above slotted groundplane, (i) resistance (ii) reactance f = 2450 MHz

The general characteristics of the impedance curves of Fig. 10 are very similar. The radiation resistance variation of the dipole over a large groundplane without a slot agrees in general with theoretical predictions for thin resonant dipoles[1]. As the slot length increases the greater absorption tends to reduce the level of the reflected power and subsequently dampen the impedance variations experienced by the dipole.

To examine the characteristics of this impedance variation when the probe wings are made short, the impedance measurements over the large groundplane were repeated with the coaxitube dipole having wing lengths of 0.194 λ and 0.111 λ. The experimental results are shown in Fig. 11. The results suggest that as the probe wing length is reduced the impedance variation due to the presence of the groundplane becomes significantly smaller. However, theoretical studies using the Hertzian dipole indicate significant variations in the impedance of a short dipole over a conducting groundplane.[9,10] The consistancy of the impedance characteristic measured on the short dipole is considered to be principly due to the swamping action of the effective shunt capacitance due to the feed configuration at the dipole imput terminals. This base capacitance plays an important role in the operation of the probe.

The voltage (V_L) appearing across the antenna load impedance Z_L is related to the incident field strength (E) by Eq. (1)

$$V_L = \frac{h_e |E| Z_L}{\sqrt{2}\ (Z_A + Z_L)} \qquad (10)$$

where h_e is the effective height defined in Eq. (5) and Z_A is the total antenna impedance including dissipation losses and any effective shunt impedance at the feed point. For useful

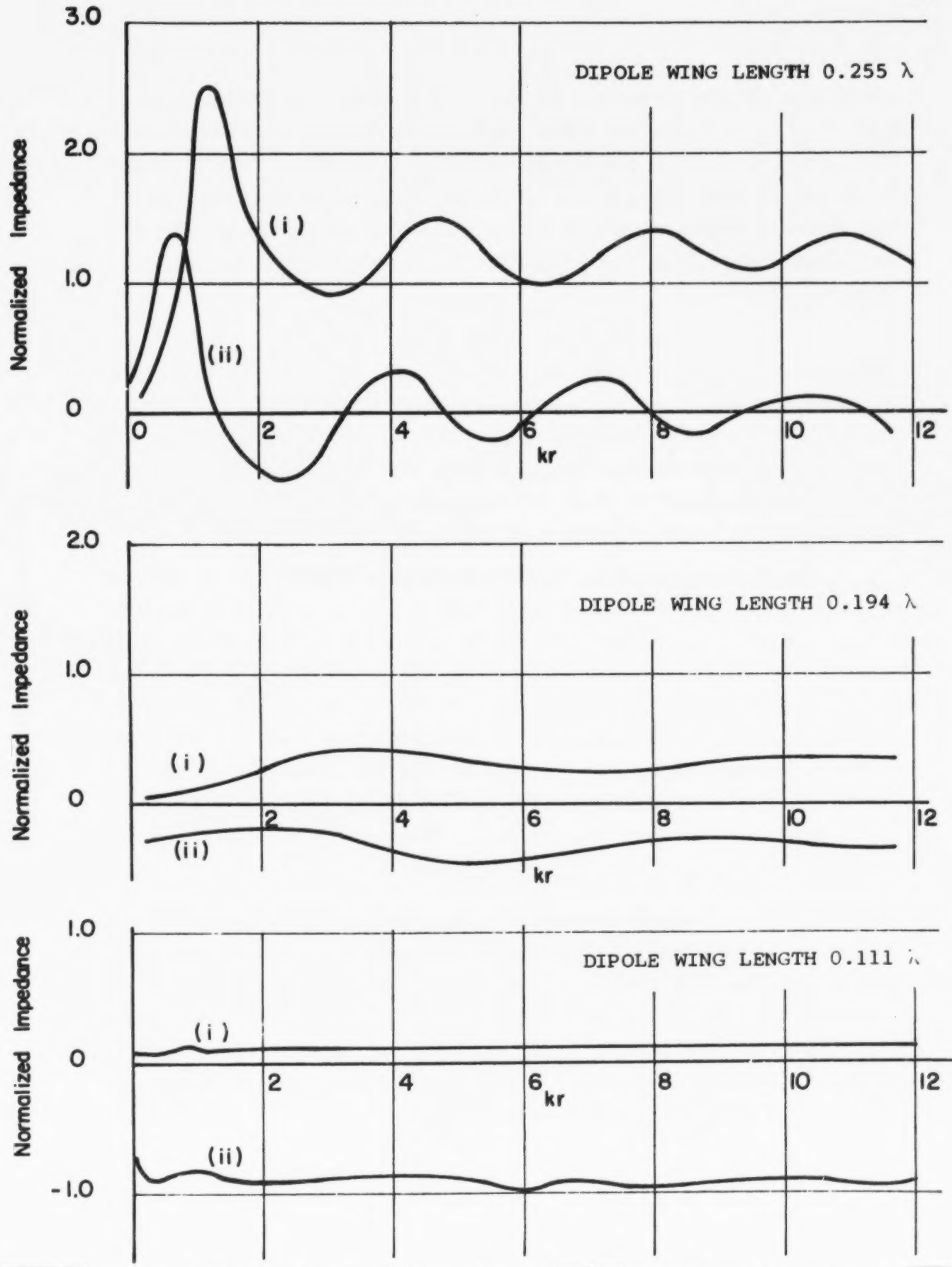

Figure 11. Variation in dipole impedance above a large groundplane for resonant and short dipoles. (i) resistance (ii) reactance f = 2450 MHz.

operation of the probe it is necessary that the ratio $h_e Z_L / Z_A + Z_L$ remain sensibly constant in the near-field region. Thus providing that the <u>total</u> antenna impedance (i.e., that measured in the experiment) does not vary significantly as the antenna approaches the large metallic object, impedance variations will not contribute to a calibration error in this region.

It is concluded, therefore, that the probe can be made insensitive to impedance variations incurred by the presence of large metallic objects provided that the probe wings are made very short relative to 0.25 λ. For such short wing probes a useful practical guide would be that the probe to object spacing be maintained greater than two overall dipole lengths for this approximation to be considered valid.

To illustrate the effect of dipole impedance variations on field measurements close to a slot in a large groundplane, Fig. 12 shows the results of field measurements approaching a 6.1 cm slot in a groundplane employing an 0.25 λ dipole probe, compared with the same probe with 0.065 λ wings. The impedance variation of an 0.25 λ dipole approaching the same slot is also shown to illustrate the correlation between the indicated field and the impedance variation for the larger dipole. The frequency of operation is 2450 MHz.

C. <u>Feed Lines</u>

The problem of conveying the measured information from the point of sensing to the necessary instrumentation hardware, without disturbing the electric field under measurement is a basic one. In this case the problem is enhanced by the fact that the resultant system must be an economical proposition. In this application an economical proposition is one costing tens of dollars rather than hundreds.

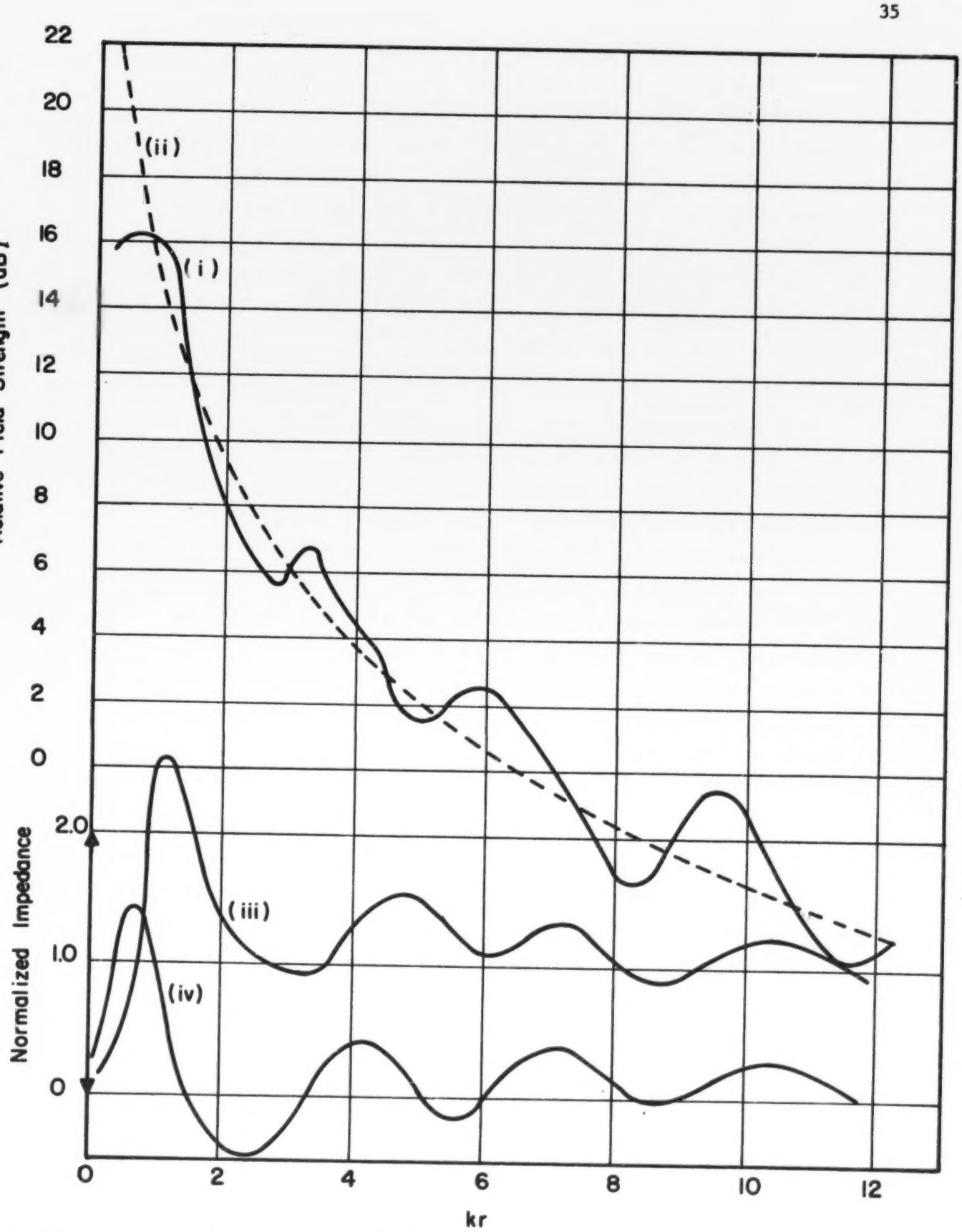

Figure 12. Illustrating effect of dipole impedance variation on field strength measurements. Field strength measurements approaching a 6.1 cm slot in a large groundplane. (i) basic probe dipole with 0.25 wings. (ii) basic probe dipole with 0.016 wings. Typical impedance variation of an 0.25 wing length dipole approaching large groundplane. (iii) resistance (iv) reactance f = 2450 MHz.

The slot fed dipole shown in Fig. 2 employs a small diameter coaxitube to pass the RF signal received at the dipole wings back to a suitable power meter. This system is only usable when the coaxitube can be positioned normal to both the plane of the dipole wings and the source aperture plane. Reduction of the coaxitube diameter provides an improvement which is limited both by constructional problems and by increasing propagation loss in the coaxitube.

For simplicity and, therefore, economy in this application there are advantages to be gained in detecting the RF signal close to the probe antenna and passing only a dc signal back to the measuring instrument - in this case a calibrated vacuum tube voltmeter (VTVM). The problem then is to construct suitable feed lines which are capable of passing a direct current while offering a poor conduction path to currents arising from an impinging RF field. The basic probe configufation of Fig. 1 restricts the RF currents from the dipole antenna to the RC circuit at the detector diode. Any RF pick-up on the dc feed wires is filtered before reaching the diode circuit by the RC components. However, it is still necessary to minimize RF current flow in the feed wires, so reducing the possibility of perturbing the field under measurement.

The use of very small diameter (i.e., 1 – 3 mils) resistance wires tightly twisted together has been found to provide one practical (although not perfect) form of feed wire. However, the wires should still be maintained normal to the plane of the dipole wings and source aperture for best results. In general, the higher the resistance per unit length of the wire the more transparent to RF the feed appears. For measurements close to radiating slots this form of feed has been found very satisfactory.

Direct current feed lines can be constructed by impregnating plastic or expoxys with carbon granules. Experimental lines were constructed using a carbon based semi-conductive lacquer and a conductive adhesive*. While these lines proved to be very effective with regard to their transparency to RF, their dc resistance was of the order of 20 - 50 KΩ/foot. Use of high impedance feed lines is undesirable in that the line tends to be noisy and also very prone to pick-up. A carbon impregnated plastic line has been reported in a National Bureau of Standards publication.(11) The line is apparently extremely transparent to RF but still has an impedance of the order of 10 - 20 KΩ/ foot.

A further experimental approach was made by depositing a thin gold film on a glass substrate. This line had a resistance of 200 Ω/foot and while it was comparatively expensive to construct showed no improvement over the twisted resistance wires.

A further possibility exists in the use of dielectric line to transmit the RF from the probe antenna to the detecting circuit, which would then be located at a distance from the point of measurement. Due to time limitations this approach was not explored during this program. However, it is hoped that the technique can be evaluated in the near future.

D. Summary

The total back-scatter introduced by the basic probe originates from the probe body, the probe antenna, and the dc feed lines. In the experimental evaluation described, the probe body, which was constructed from a low dielectric constant material, and the very small detection circuit components, were not found to contribute significantly to the back-scatter.

---

*Eccocoat and Eccobond by Emerson Cumming, Inc.,

The major source of scattering was found to be that due to the probe antenna, particularly when the dipole wing lengths were of the order of 0.25 λ. The magnitude of the scattered power was found to be a function of the length of the dipole wings and the load on the wings. Theory indicates[3,5] that the level of the antenna back-scatter can be reduced by reduction of the antenna wings with an associated reduction in antenna gain. This was substantiated in the measurements.

Reduction of the back-scatter can be achieved by using a very small reactive antenna providing the detection sensitivity is sufficient. When this is so the probe can be used very close to a radiating source or a large metallic geometry without multiple coupling effects or probe impedance variations disturbing the electric field free space calibration factor. However, other factors have yet to be considered in the following sections with regard to both electric field strength and power density calibrations.

By detecting the RF signal close to the probe antenna the feed line problem becomes one of providing a dc path which is, as nearly possible, transparent to RF. Very small diameter twisted resistance wire feed lines were found to be a practical approach providing the wires were maintained normal to the plane containing the dipole wings and the source aperture. The higher the resistance per unit length the more transparent to RF the wires appear.

Other forms of "transparent" dc feed lines, such as carbon impregnated expoxies, were found to be suitably transparent to the RF field regardless of orientation. However, these feed lines have a very high dc resistance (20 - 50 KΩ/foot) and thus demand very high impedance metering circuits which tend to be more susceptible to both self generated, and pick-up noise. A National Bureau of Standards report[11] mentions a similar probe feed line constructed by impregnating a plastic line with carbon. Again the dc resistance tends to be high (10 - 20 KΩ/foot).

VIII. FIELD CURVATURE

In a near-field measurement, even in the absence of scattering effects the effective height of the probe dipole antenna may be subject to variation due to curvature in the wavefront of the incident electric field. To examine this variation we shall consider a worse case slot situation when the probe antenna approaches a single magnetic current element in an infinitesimal slot, located in an infinite groundplane.

From Eq. (5) the dipole effective height can be expressed as

$$h_e = -\int_{-h}^{h} i(x)\ e(x)\ dx \qquad (11)$$

where "i" is the current distribution along the dipole (oriented along the "x" axis) normalized to its value at the input terminals and "e" is the component of the incident electric field tangential to the surface of the dipole, normalized to its value at the center of the dipole, and "h" is the physical half length of the dipole.

In terms of the angular co-ordinates of Fig. 13a and assuming a short thin dipole the normalized current distribution along the dipole may be approximated by

$$i = \left(1 - \left| \frac{\tan \Downarrow}{\tan \Updownarrow} \right| \right) \qquad (12)$$

where $\Updownarrow = \tan^{-1} \frac{h}{r_o}$.

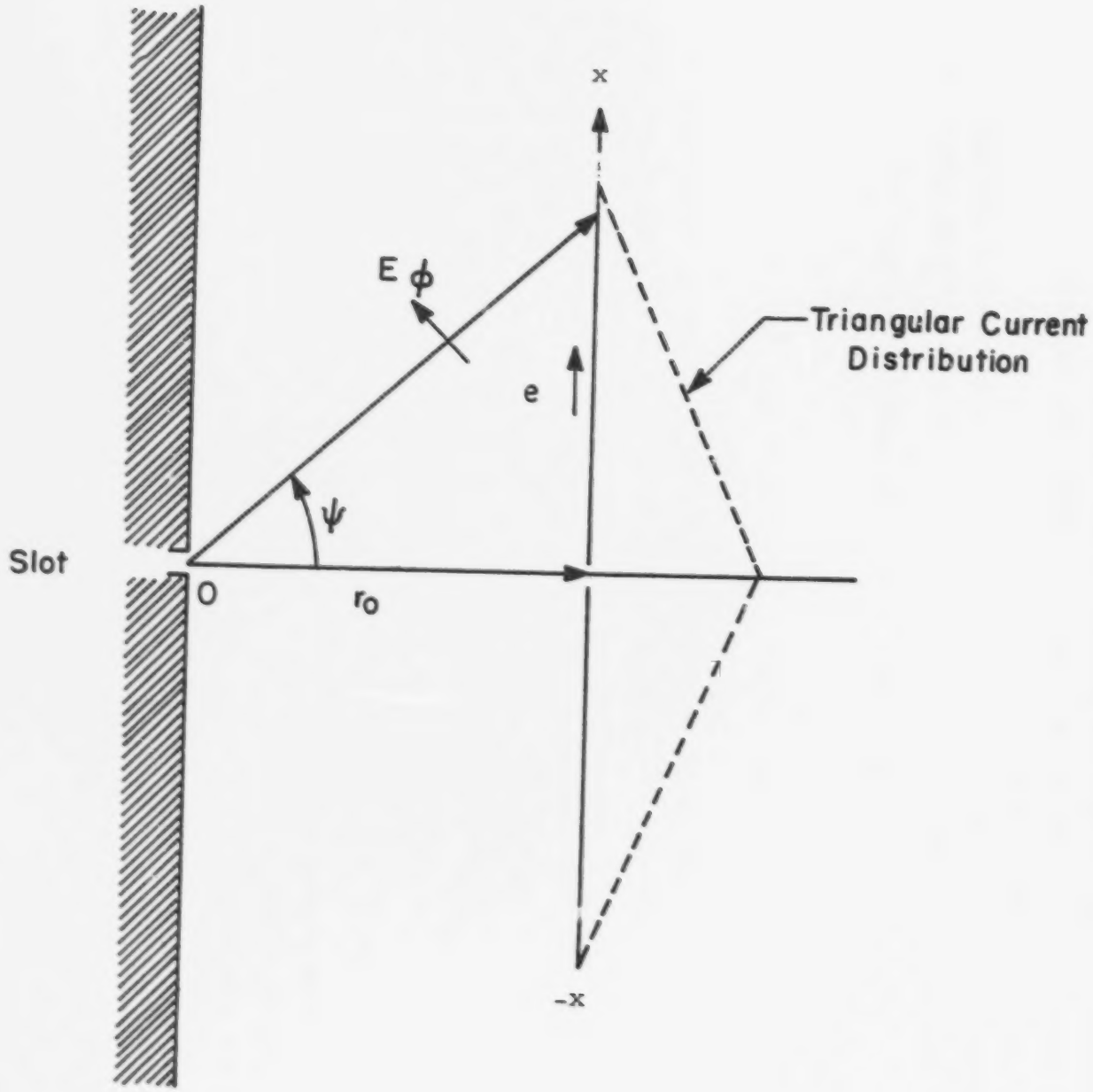

Figure 13. (a) The nomenclature for the "effective height" (h_e) calculation.

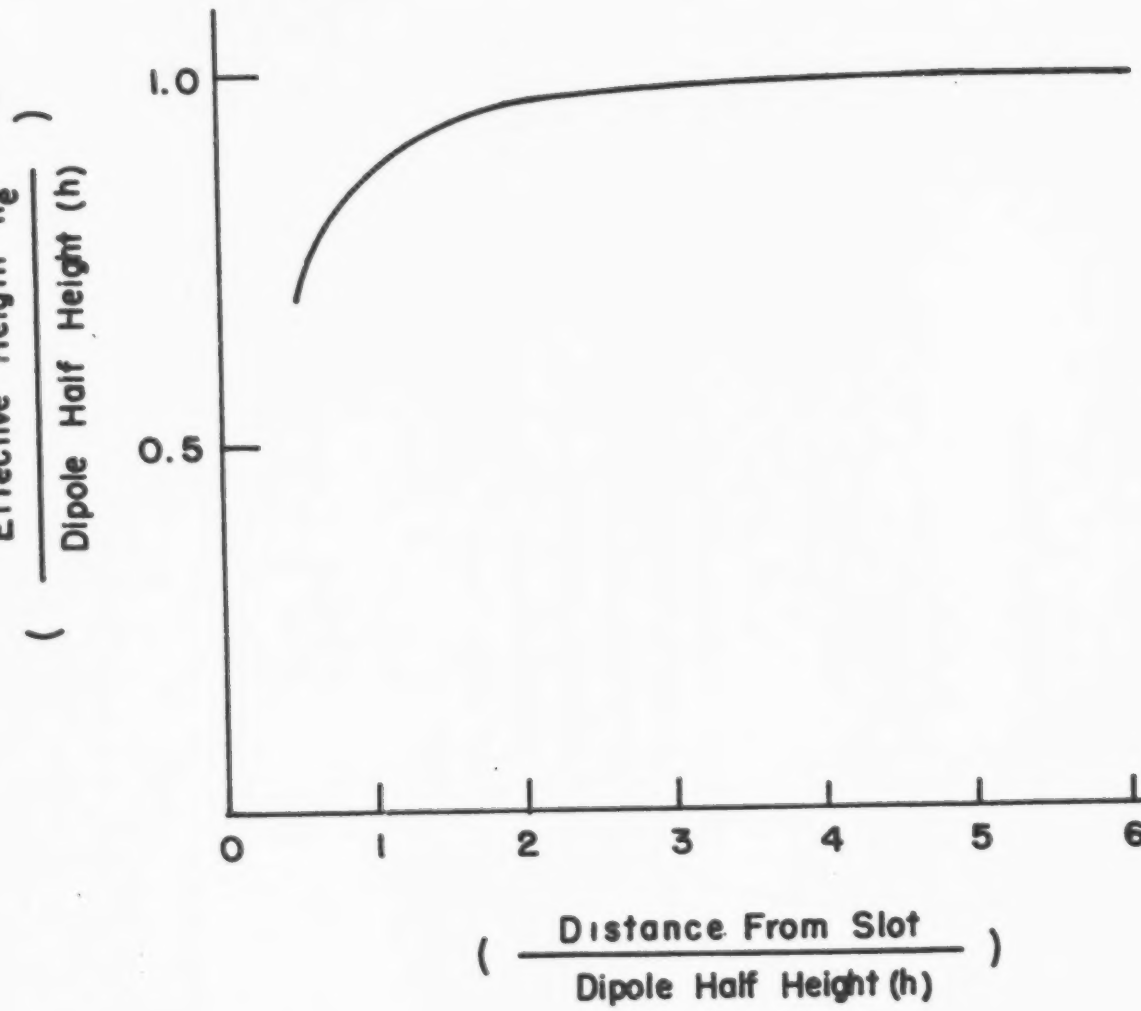

Figure 13. (b) The variation of $(h_e)^2$ as the probe approaches the slot.

The normalized component of the tangential electric field at the dipole may be expressed from the geometry of Fig. 13a as

$$e = \cos \psi \exp(jkr_o \sec\psi) \tag{13}$$

where $k = 2\pi/\lambda$.

Equation(11) may then be written

$$h_e = 2r_o \int_0^{\hat{\psi}} \left(1 - \left|\frac{\tan \psi}{\tan \hat{\psi}}\right|\right) \sec \psi \exp (jkr_o \sec\psi)\, d\psi \tag{14}$$

In the preceding sections we have shown that the impedance variation of the probe antenna can be kept to an insignificant level providing the probe does not approach within a few "overall dipole lengths" of the source, or a conducting surface. Hence, we are largely concerned with the effect on h_e for values of ψ less than 45°, and it is sufficient to evaluate

$$h_e = 2r_o \int_0^{\hat{\psi}} \left(1 - \left|\frac{\tan \psi}{\tan \hat{\psi}}\right|\right) \sec \psi \, d\psi \tag{15}$$

Integrating gives

$$h_e = 2r_o \left\{ \log_e \tan\left(\frac{\pi}{4} + \frac{\hat{\psi}}{2}\right) - (\operatorname{cosec} \hat{\psi} - \cot \hat{\psi}) \right\} \tag{16}$$

In Fig. 13b $(h_e)^2$ is shown normalized to the physical half length (h) of the dipole.

From Fig. 13 it can be concluded that the variation in effective height due to field curvature can be assumed to be negligible providing that the probe antenna does not approach a source or boundary closer than 2 or 3 overall dipole lengths (i.e., 4h to 6h).

IX. POWER DENSITY CALIBRATION

The preceding examination of multiple coupling, dipole impedance variation and effective height has indicated that while these effects can introduce errors in the probe far-field calibration factor, the probe will maintain its free space calibration with regard to an electric field strength measurement providing the physical height of the dipole is made very small with respect to the operating wavelength and that the back-scatter from the probe body and feed is reduced to a very low level with respect to the incident field. With these provisions accurate electric field strength measurements can be made as close as two or three overall dipole lengths from a source or boundary region employing a free space calibration factor.

Assuming, therefore, that the electric field can be measured accurately, it is necessary to determine to what extent the conversion of this measurement to a power density indication via a constant calibration factor can be considered accurate.

In the derivation of the free space effective aperture calibration factor in Section II the wave impinging on the antenna was considered as purely TEM with a wave impedance given by $E/H = Z_o$, the free space impedance. In a region close to an electromagnetic source or boundary the modal structure of the field will be undergoing a transition between that of the source and that of free space. Hence, the approximation implied in Eq. (3) cannot be considered valid in the region.

To obtain some insight into these effects two source configurations will be considered. The first is that of a narrow slot in a metallic groundplane. This is primarily a TE mode source and is typical of many radiation leakage situations. The second is the electric dipole, which is predominantly a TM source and while it is not quite as common

as a source of radiation leakage, it does introduce additional problems in the conversion of electric field measurements to a power density indication.

The field distribution along a slot in a large groundplane may be described theoretically by a weighted line distribution of magnetic current elements,[3] the weighting function being directly proportional to the slot voltage distribution. The contribution from each elemental magnetic current to the field distribution at a point in the near-field may be expressed in scalar form with the notation of Fig. 14 as[3]

$$dE_\phi = -\frac{ae_m}{2\pi} f(x)dx\, e^{-jkr}\left(\frac{jk}{r} + \frac{1}{r^2}\right)\cos(n,r) \qquad (17a)$$

$$dH_\theta = \frac{ae_m}{2\pi Z_o} f(x)dx\, e^{-jkr}\left(\frac{jk}{r} + \frac{1}{r^2} - \frac{1}{kr^3}\right)\cos(n,r) \qquad (17b)$$

$$dH_r = \frac{ae_m}{2\pi Z_o} f(x)dx\, e^{-jkr}\left(\frac{2}{r^2} - \frac{2j}{kr^3}\right)\cos(i,r) \qquad (17c)$$

where e_m is the maximum slot field strength, $k = 2\pi/\lambda$, $f(x)$ is a normalized complex function describing the voltage distribution along the slot, $\vec{n}$ is a unit vector normal to the plane of the slot, $\vec{i}$ is a unit vector in the x direction, and $\cos(n,r)$ and $\cos(i,r)$ are the directional cosines. The e^{jwt} time factor has been suppressed.

The complex Poynting vector for this case will have two components. The complex power flow (P_c) will be given by

$$P_c = E_\phi H_\theta^* + E_\phi H_r^* \qquad (18)$$

The second term in Eq. (18) is a purely reactive power flow,

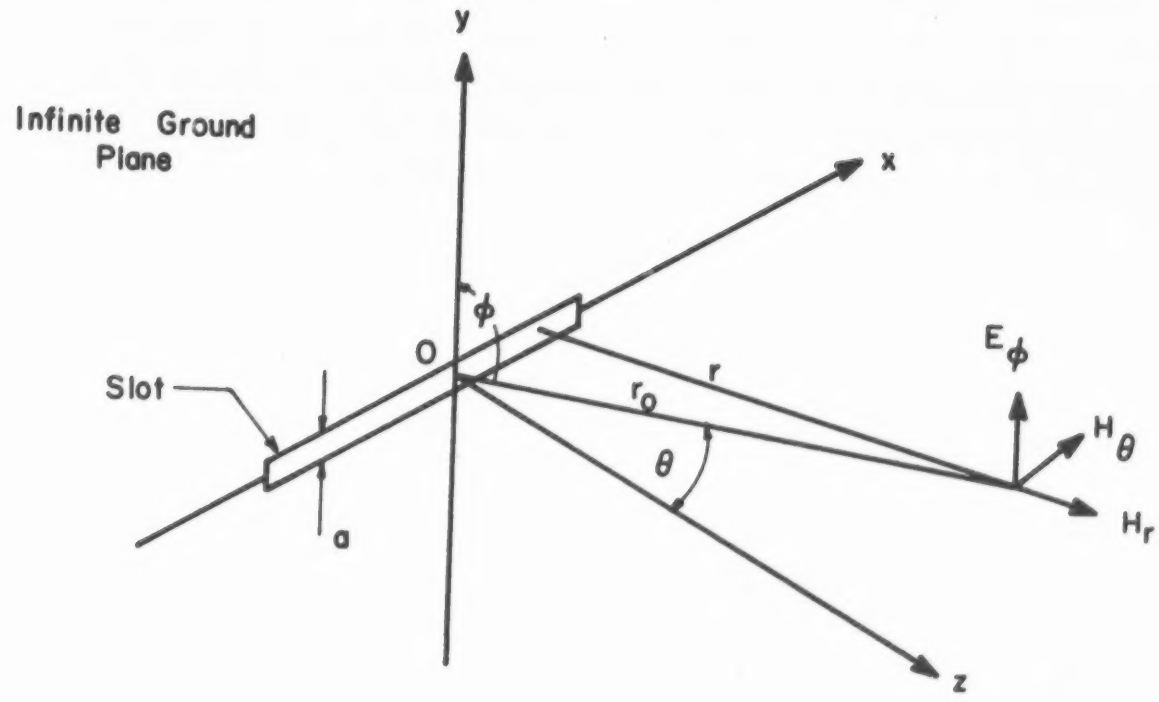

Figure 14. Coordinate system for the case of a slot in an infinite groundplane.

radiating no power to the far-field and thus it's average Poynting vector will be zero. Hence, the average power flow, as given by Eq. (2) will be

$$P = 1/2\ R_e \left\{ E_\phi H_\theta^* \right\} \tag{19}$$

Solutions to the integrals implied in Eq. (17) (for E_ϕ and H_θ) are difficult to obtain analytically and the value of any one solution is restricted to the particular slot voltage distribution expressed in f(x). However, consider the field distribution at a point in the near-field due to a single elemental magnetic current element located at a point on the slot. At this point the ratio of E_ϕ/H_θ due to the elemental magnetic current will be

$$\frac{E'_\phi}{H'_\theta} = Z(r) = \frac{Z_o\left(\frac{1}{kr} - \frac{j}{(kr)^2}\right)}{\left(\frac{1}{kr} - \frac{1}{(kr)^3} - \frac{1}{(kr)^2}\right)} \tag{20}$$

From this equation it can be seen that only the presence of the cubic term in the denominator makes Z a function of "r", and as "r" increases the expression for Z rapidly approaches Z_o.

The cubic term appears as a result of H_θ (see Eq. (17)). With a practical slot having an arbitrary voltage distribution the value for H_θ at a point in the near-field will comprise of the integral of weighted contributions from all parts of the slot. However, it can be seen from Eq. (17) that regardless of the form taken by f(x), the cubic term $1/(kr)^3$ will always be accompanied by a term 1/kr, and from contributions from points further along the slot the increase in "r" will result in a decrease in the significance of the cubic term in the total integral. It can, therefore, be deduced that

worst case (i.e., slot distribution providing the largest relative cubic component) will be that of a single magnetic current element, or $f(x) = \delta(x)$ where $\delta(x)$ is the Dirac delta function.

While such a slot distribution is not physically realizable, it can be approached by a very short slot or a longer slot with a single peak in its voltage distribution. Its value in this case is that it represents a worst case with regard to the average power density indicated by the electric field probe with far-field calibration, as compared with the average power density indicated by Eq. (2).

To illustrate the effect of the cubic term in close proximity to the slot, Fig. 15 shows the ratio of the average power densities indicated by the electric field probe to those given by Eq. (2), at decreasing probe-slot spacings, for the cases of $f(x) = \delta(x)$ (very short slot) and $f(x) =$ constant (very long slot). The probe is assumed to measure the electric field accurately and to have a free space calibration such that the power density is given by Eq. (3).

Figure 15 shows that the electric field probe will err by an increasing factor as the probe approaches the slot. The error being such that a power density higher than that given by the average of Poynting's vector will be indicated by the probe. It is not proven that any arbitrary slot distribution will produce an error curve lying between the given curves, although intuitively it would seem likely, but any other error curve will be below the worst case value given by $f(x) = \delta(x)$. Uniform slot distributions will approach the long slot case except at regions of discontinuity at the slot ends.

To given some experimental support to the results shown in Fig. 15 measurements of power density were made with a small electric field probe approaching along the normal to the center of a narrow slot 0.245 λ long in a large groundplane (see Fig. 5).

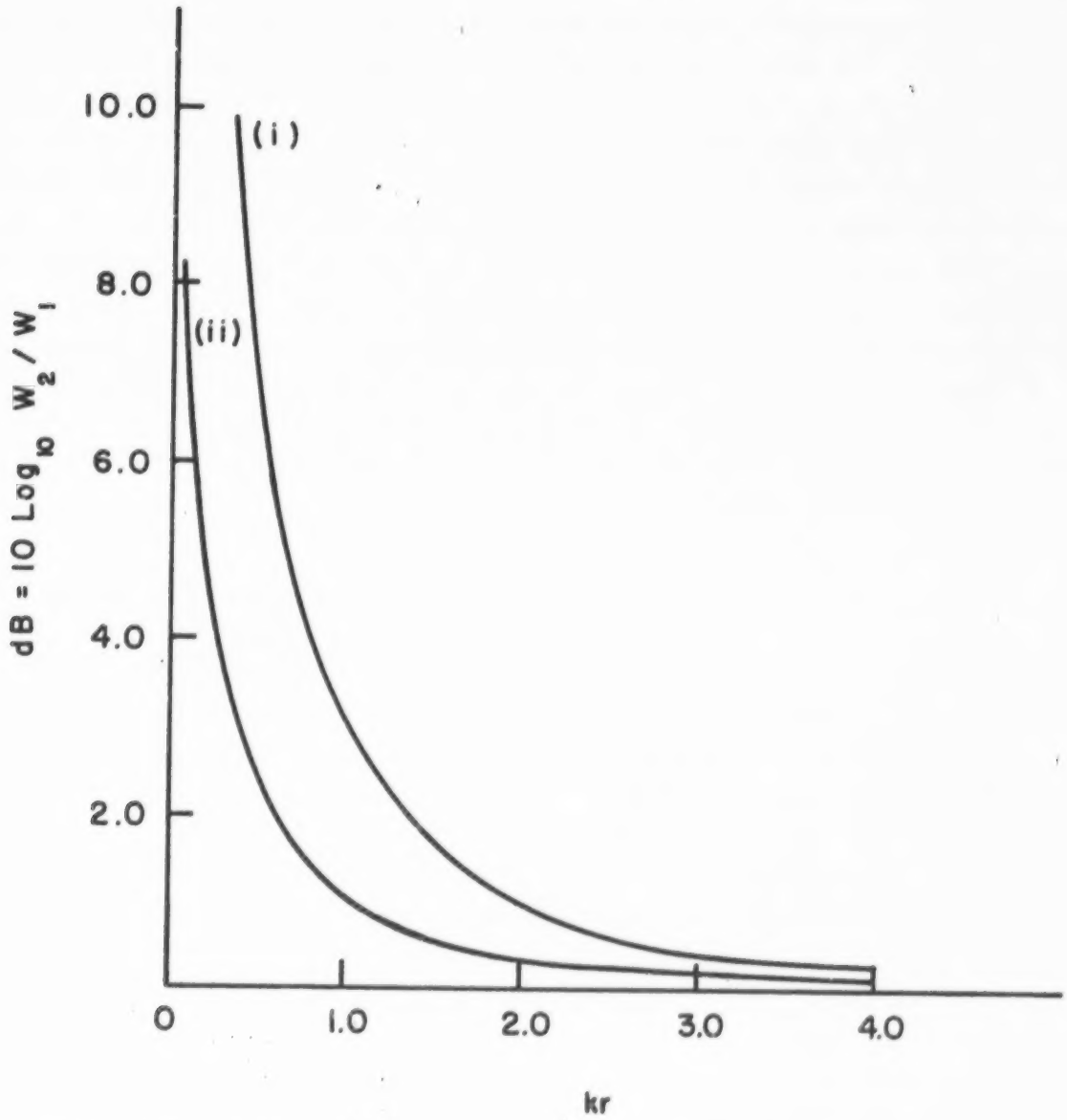

Figure 15. Ratio of $\frac{(W_2)}{(W_1')}$ where W_2 = average power density indicated by electric field probe

W_1' = average power density given by 1/2 R_e $(\vec{E} \times \vec{H})$

as probe approaches a slot in a large groundplane.
(i) a very short slot (ii) a long uniform slot field distribution

Measurements of power density indicated by the probe are shown in Fig. 16 superimposed on the power density indicated by Eq. (2) for an elemental slot length. The physical slot ceases to look like the elemental (point source) slot as the angle subtended by the ends of the slot to the point of measurement becomes larger. The reduction in real power density with distance from the 0.245λ slot will thus approach the square law of the elemental slot at distances corresponding to $kr > 1.0$ and will be less than square law in the region $kr < 1.0$. The tendency for the probe to indicate high is clearly shown. In the region $kr < 1.0$ the probe indicates that the power density is increasing at a rate greater than the square law associated with an elemental slot. For probe to slot spacings greater than $\lambda/2\pi$ the calibration error shown by Fig. 16, (i.e., between the probe power density indication and that given by Eq. (2)) is in good agreement with that predicted by the potential error curve given in Fig. 15.

The curves shown in Fig. 15 indicate the limitations of the far-field power density calibration for electric field probes making accurate electric field strength measurements close to radiation slots. An error of up to 3 dB may be involved in a slot and groundplane configuration when the probe to slot spacing is $\lambda/2\pi$. This potential error could be expressed as $\pm$ 1.5 dB by use of a suitable calibration correction factor.

Although TE mode sources, such as slot radiators, are more typical of the situations which may be encountered in near-field hazard measurements, TM mode sources, such as the electric dipole, raise further difficulties. In the near-field of a TE mode source there is no component of the electric field in the direction of propagation. With a TM mode source such a component of electric field exists and although this component decays rapidly away from the source, in the near-field region its magnitude is comparable with that of the transverse field.

The electric field component in the direction of propation is associated with a purely reactive power, nevertheless, if the near-field probe antenna is oriented such that its antenna is excited by this field component, then the probe output will erroneously indicate a real power flow. The level of this apparent power flow relative to that indicated by

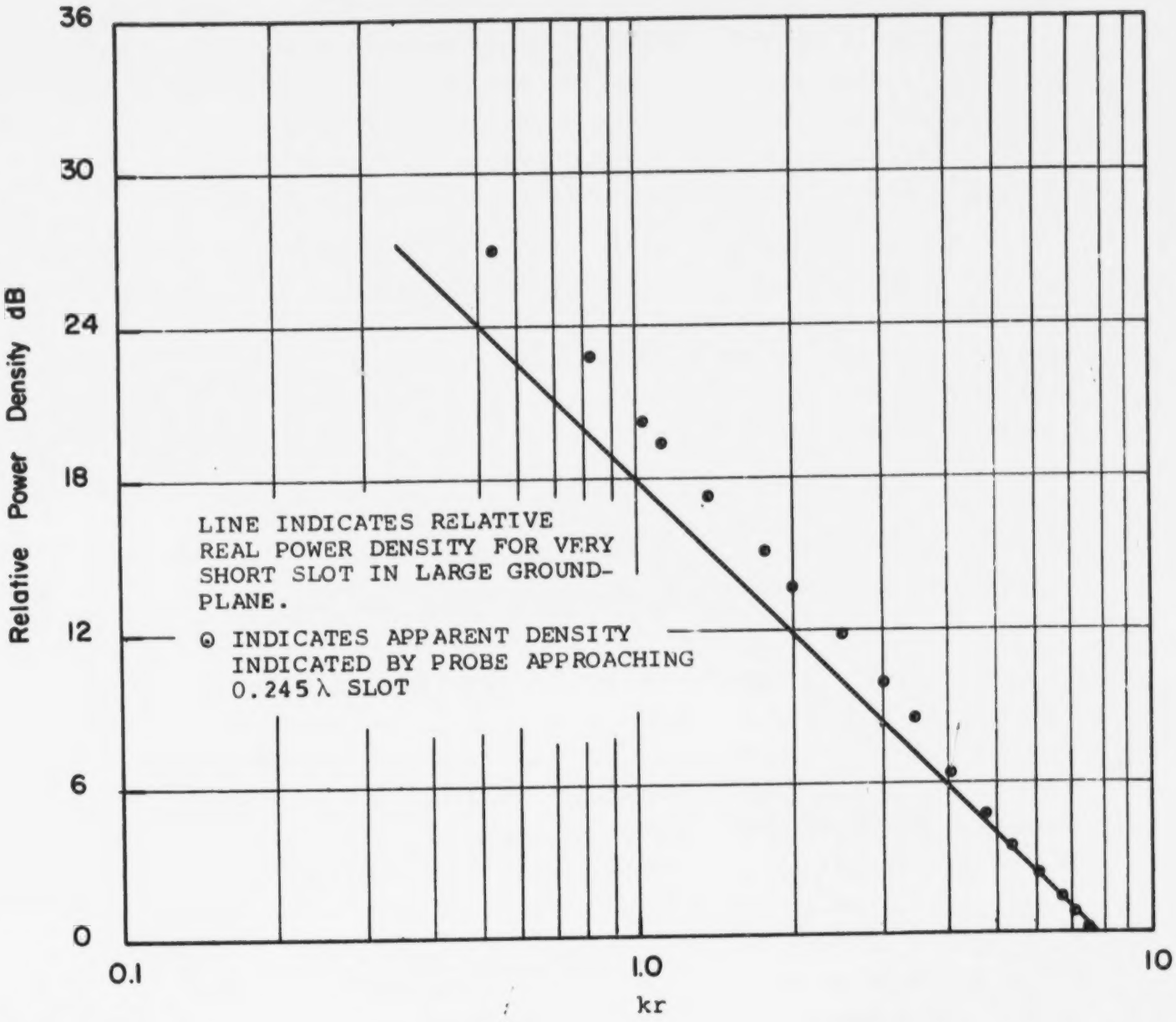

Figure 16. Experimental data supporting the potential error curves of figure 15.

the transverse field component for a small current element source is shown in Fig. 17. The second curve shows the ratio of this apparent power flow to the true power flow for the same current element source. The difference between these curves when kr is small indicates that, as for the case of the radiating slot source, the electric field probe power density calibration is in error close to the source, even when the probe is correctly oriented to receive only the transverse field.

To illustrate this power density calibration error Fig. 18 shows a worst case example as the electric field probe approaches a small elemental current source. The curves indicate the ratio of the power density indicated by the probe relative to the power density given by Eq. (2) for (a) an elemental current source and (b) a long uniform current distribution. Superimposing the curves of Fig. 18 upon those of Fig. 15 provides a guide to the potential power density calibration error in accurate electric field probes approaching TE or TM mode sources providing the probe antenna is aligned with the transverse field component.

Drawing some practical guidelines from these results it would appear that a far-field power density calibration on an accurate electric field strength probe will be less than 3 dB in error at probe-source spacings greater than $\lambda/2\pi$ for practical source configurations of the type considered providing the probe antenna is aligned correctly with the transverse field. This could be expressed as ± 1.5 dB with a near-field calibration correction. For TM sources an incorrectly oriented probe can lead to apparent power density indication from a purely reactive field. In this case, a probe to source spacing of greater than $2.2\lambda/2\pi$ is required to ensure that the peak value of the apparent power density is not greater than the real power density at the same point.

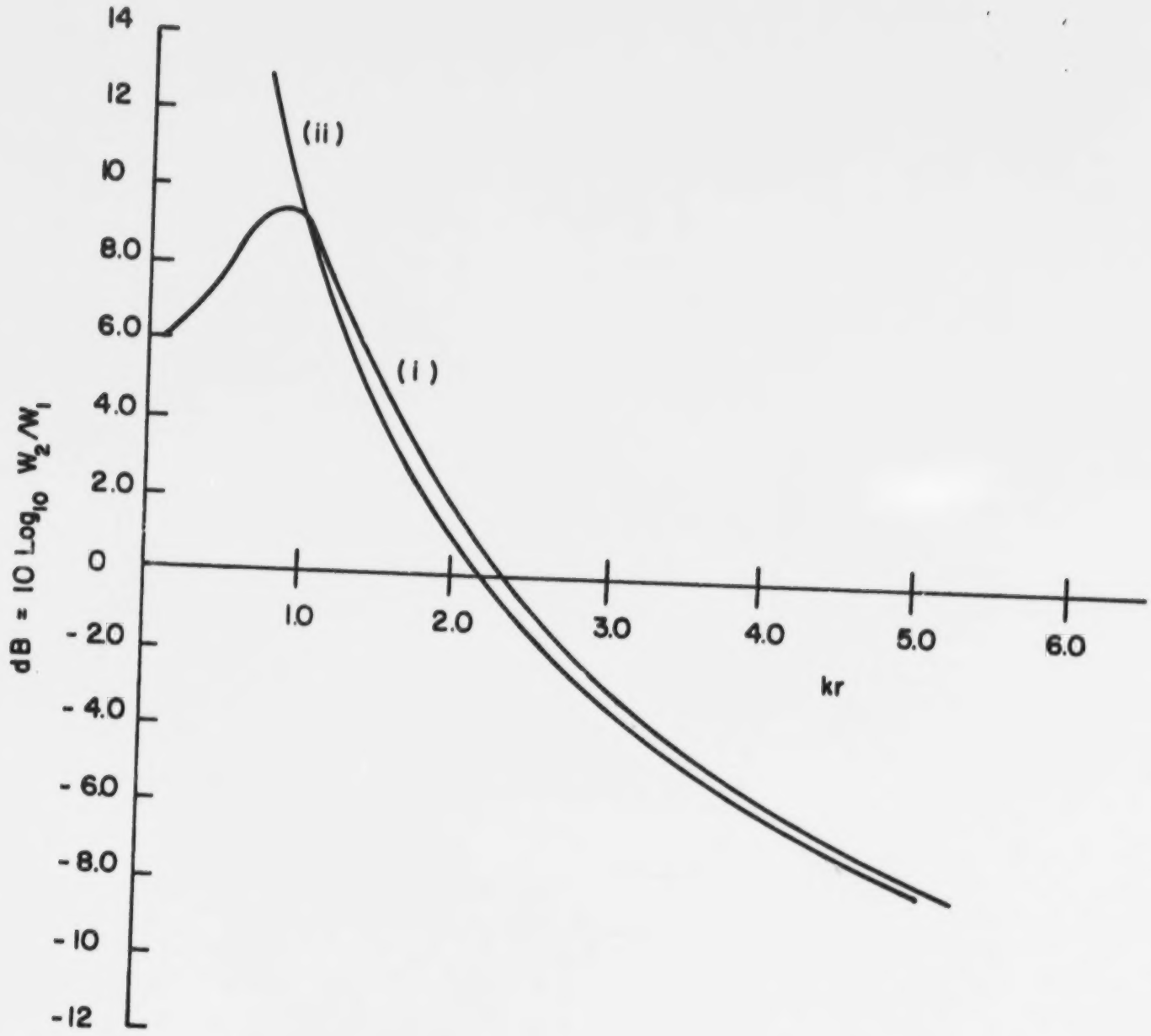

Figure 17. With electric field probe approaching a single current element (T.M. source).

(i) Ratio of $\frac{(W_2)}{(W_1)}$ (ii) $\frac{(W_2)}{(W_1')}$

where W_2 = apparent power density indicated by probe due to purely reactive field component

W_1 = apparent power density indicated by probe due to transverse field component

W_1' = power density given by $1/2\ R_e\ (\vec{E} \times \vec{H})$

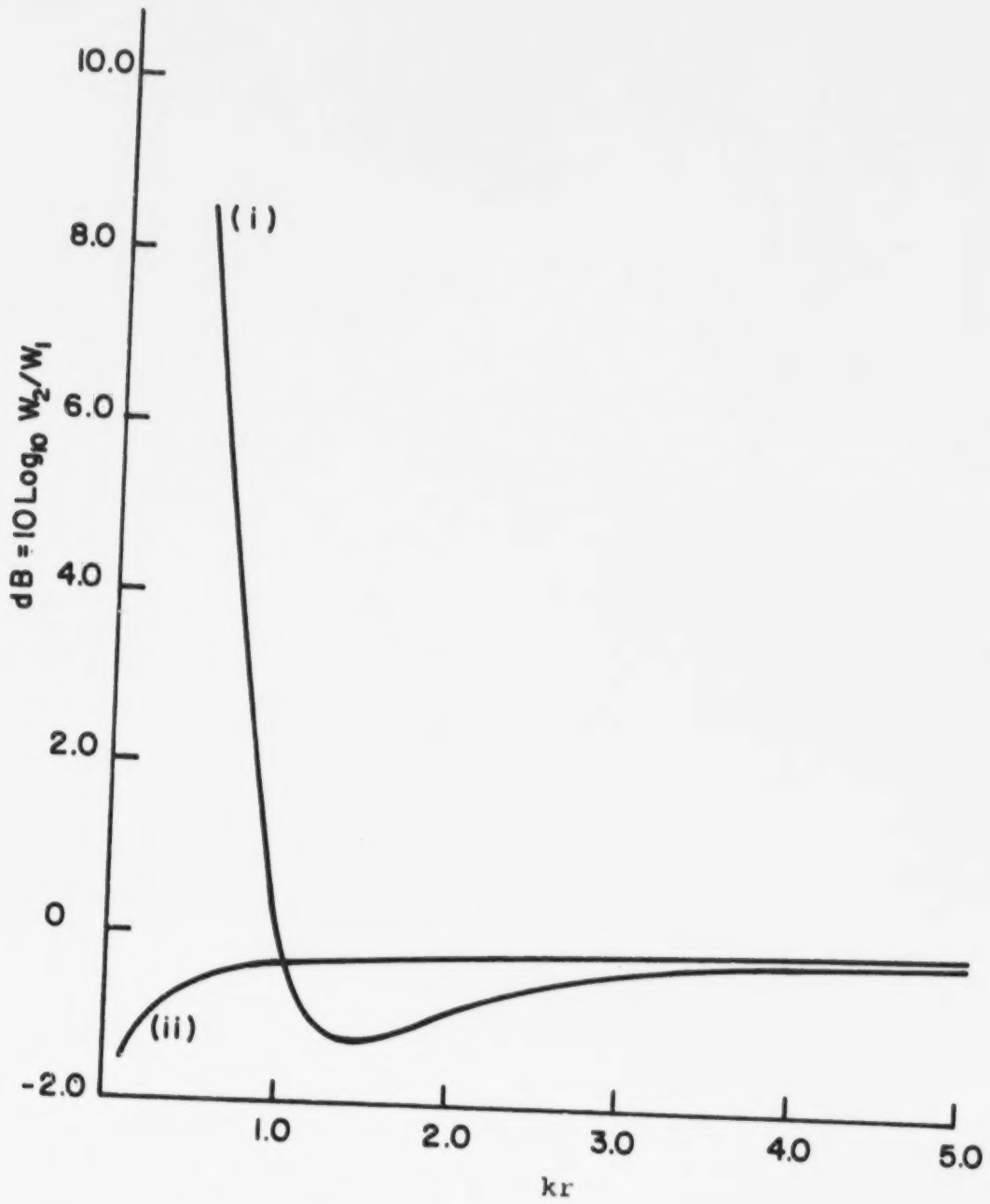

Figure 18. Ratio of $\frac{(W_2'')}{(W_1')}$ where W_2'' = apparent average power density indicated by electric field probe

W_1' = average power density given by $1/2\ R_\varepsilon\ (\vec{E} \times \vec{H})$

as probe approaches (i) a single current element
(ii) a long uniform current distribution

X. PROBE POLARIZATION

For operational convenience it is desirable that the near-field probe be insensitive to the polarization of the incident energy. Although the basic probe configuration of of Fig. 1 is linearly polarized, experimental work has shown that an orthogonal "crossed dipole" arrangement can achieve the required polarization performance. Measurements on the basic probe configuration reveal that even when the dipole wings are made extremely short the mutual coupling effects between orthogonal dipoles is small. The summation of the output contributions from the orthogonal dipoles can be carried out either in the RF circuit, when a suitable phasing circuit is required, or in the dc circuit, when two detector diodes are necessary.

In view of the fact that with the very short wings employed the diode itself is virtually the dipole antenna, the dc summation was chosen as one offering the most simple physical layout. Figure 19 illustrates the arrangement. With the very short wing lengths employed in the probe the presence of the body of the front diode tends to reduce the sensitivity of the rear diode. This effect may be compensated in two ways. The wing length of the rear diode can be increases slightly or the sensitivity of the front diode can be reduced by reducing its wing length or adding a small capacitance in parallel with the diode.

The silicon diodes employed were found to have more than adequate sensitivity and thus in general the latter solutions were found most suitable. The shunt capacitance was constructed by connecting a 1.0 mil insulated wire to each end of the front diode and twisting the two ends together. The capacitance is adjustable by the number of turns and their tightness. When the right order of capacitance was found the wires were sealed into position with plastic cement, and fine sensitivity adjustments made by clipping the dipole wings.

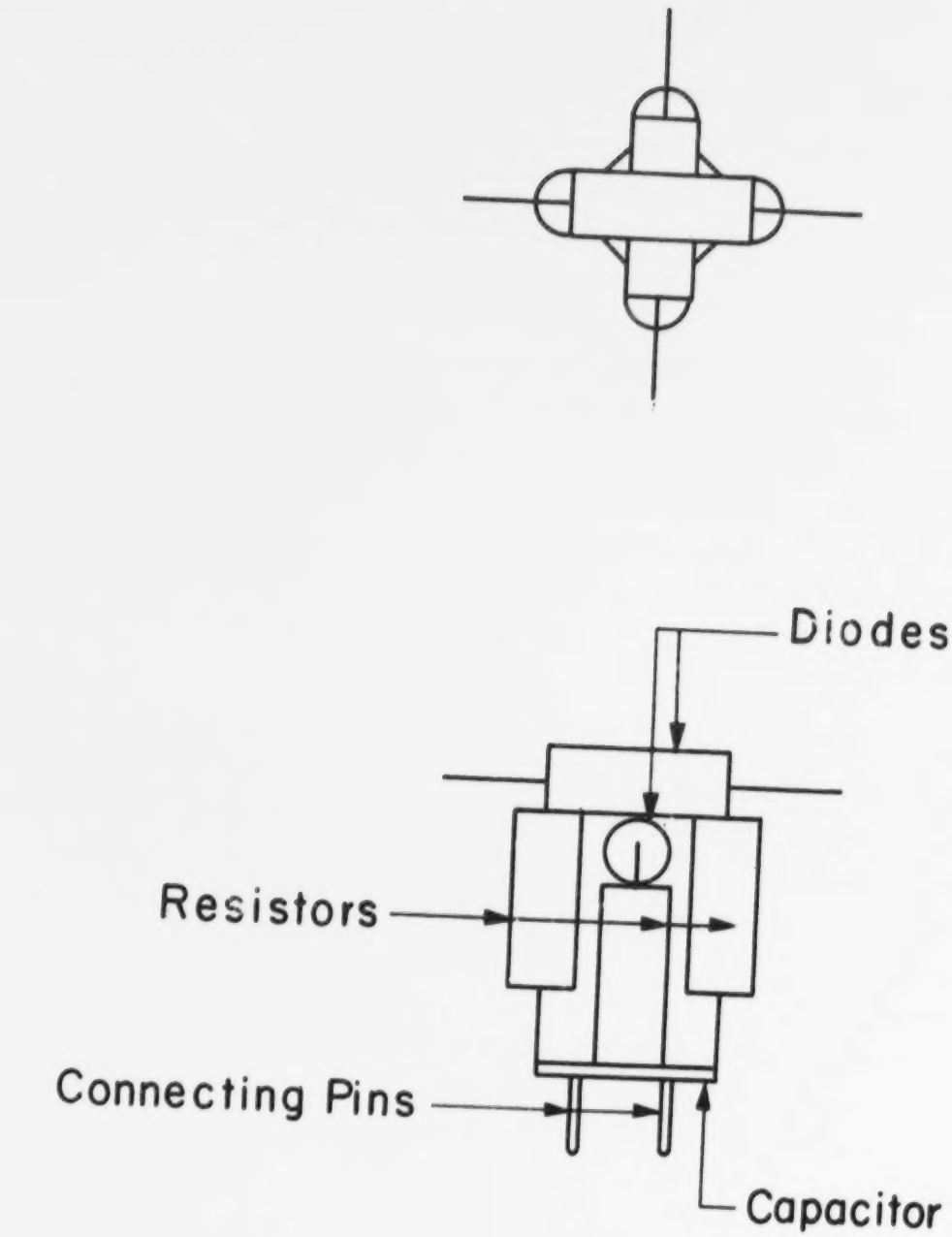

Figure 19. The crossed dipole-diode configuration.

To maintain the pre-set elipticity ratio over the large dynamic range required, it is necessary that the diodes employed be a matched pair. The matching should be such that the sensitivity of the diodes in terms of "voltage out" versus "power in" should be closely similar in the range - 50 dBm to - 10 dBm. The elipticity ratio is defined by the maximum to minimum probe output when the probe antenna is rotated about the axis normal to the plane of the dipole wings.

XI. FINAL FORM OF THE PROTOTYPE PROBE

The design features of the final prototype probe are illustrated in Fig. 20. The body of the probe is constructed from "low K"* a material having a relative dielectric constant of 1.8. This material was found to be virtually transparent to the RF fields. The general configuration and choice of dimensions of the probe body is very flexible. The prototype configuration was chosen for robustness while maintaining the feed lines normal to the plane containing the dipole wings (see Section VII.C). A much smaller body diameter could be used if required, although in this case it is necessary to ensure that the dc feed lines contained within the probe body do not lay too close to a conducting medium during the measurement. (A clearance of 0.25 inches was found to be more than adequate in the experimental work and much smaller separations are probably tolerable.)

The dc feed lines within the probe body are comprised of a pair of tightly twisted insulated resistance wires with a diameter of 2 mils and a resistance of 30 ohms per foot. The wires were fed through a small hole along the axis of the probe body to ensure that they were maintained normal to the plane containing the dipole wings (see Sections VI and VII.C).

At the rear of the probe a 4 foot long flexible feed line is provided to connect the probe to the control box. The core of the flexible dc feed line consists of a pair of tightly twisted, small diameter, insulated wires. The wires are protected from the close proximity effects, discussed in Section VI, by encasing them initially inside several layers of plastic "spaghetti" and finally within an 0.5 inch diameter flexible plastic tube. This simple arrangement was found to provide very good protection against pick-up noise and noise levels of less than 32 microvolts were easily achieved (see Section VI).

---

*Manufactured by Emerson Cumming, Inc.

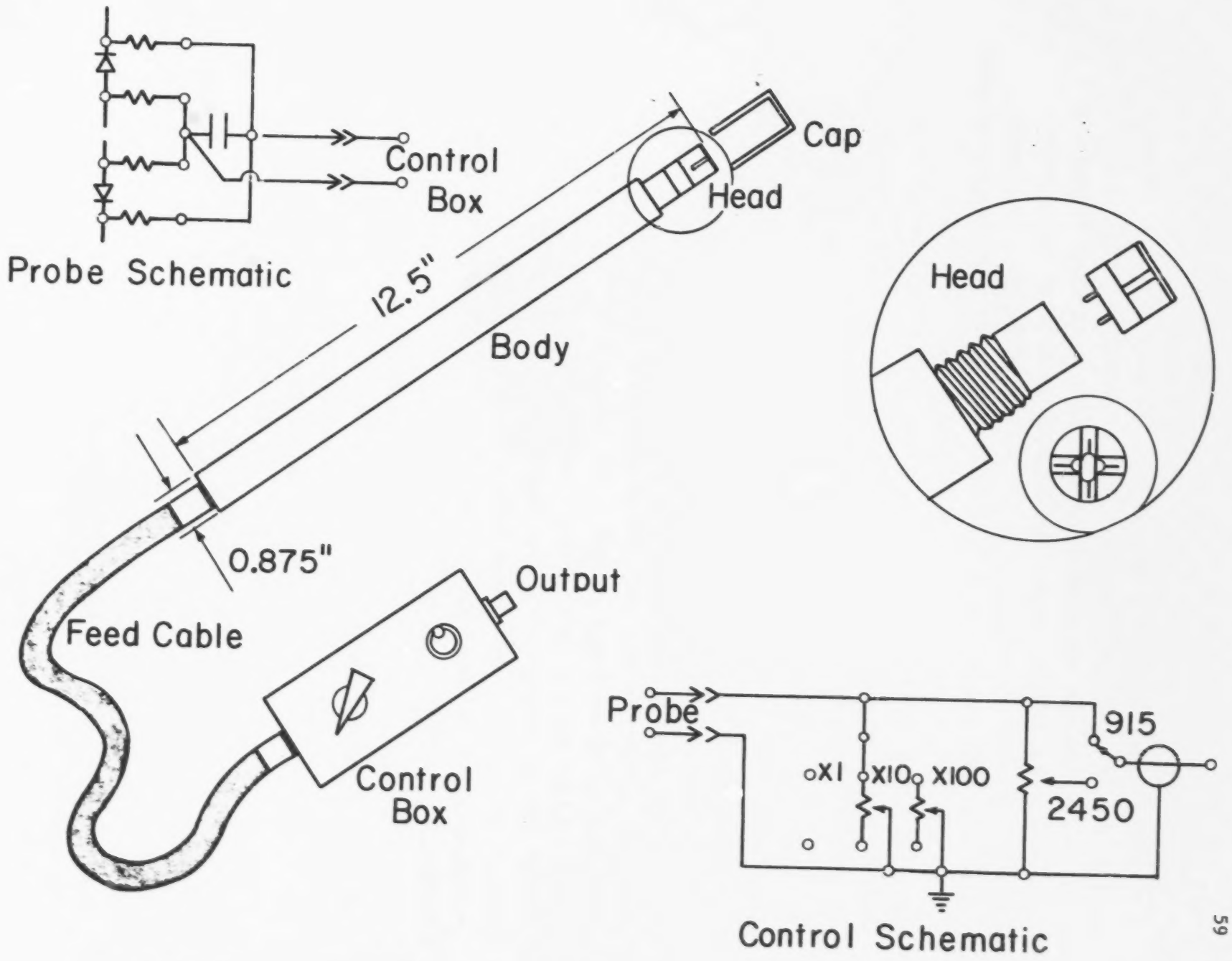

Figure 20. The prototype probe.

The control box, shown in Fig. 20, contains the range switch and the frequency calibration selector switch. The range switch merely selects a suitable value of load resistance to prevent the larger output voltages from driving the diode from its square law characteristic (see Section VI). The upper range load resistances (i.e., "MID" and "HIGH") are potentiometers which are adjusted to provide "XI0" and "XI00" range factors over the "LOW" position. Using the approach outlined in Section VI the potentiometer values selected were 0 - 1 KΩ and 0 - 100 Ω, respectively.

In the "LOW" position the dc load on either diode is largely that of the detector components and the back resistance of the other diode. To adjust the potentiometers the output on the "LOW" range is set to a full scale value of 10 mV by placing the probe in a suitable field intensity. Switching to "MID" range the relevant potentiometer is adjusted to divide this output by a factor of ten. The field intensity is then increased to give a full scale reading of 10 mV on the "MID" range and switching to "HIGH", the second potentiometer can be adjusted to divide this output by a further factor of ten. The resistance values obtained, using this procedure on the prototype probe, were "MID" range 650 ohms, "HIGH" range 57 ohms.

To allow for some discrepancy in the calibration factor on the two operating frequencies specified, i.e., 2450 MHz and 915 MHz, a third potentiometer was included in the control box circuitry. A 1.0 Megohm potentiometer was employed to avoid loading the diode output to a significant degree. The probe voltage output at 2450 MHz was expected to be somewhat greater than that obtained at 915 MHz, for the same field intensity. Hence, in the 2450 MHz position the output port of the control box is switched to the slider of the potentiometer to allow equilization of the output voltage, and thus permit a common calibration factor (in mW/cm^2 per mV of probe output) at either frequency.

The respective calibrations at 2450 MHz and 915 MHz were found to differ by only 10% -- an indication of the broadband potential of the prototype probe. The potentiometer was employed to equilize the output although it appears very probable that with further effort the calibration selector switch could be made redundant.

The probe head, which is accessible after unscrewing the protecting cap, contains the antenna and the detection components and is a "plug in" unit. The "plug in" feature was incorporated to provide some flexibility in view of the experimental nature of the probe, although such a feature also has long term advantages in that the detector circuitry can be more simply replaced. The probe antenna uses a crossed dipole configuration and obtaines the required polarization insensitivity by use of a dc summation employing two detector diodes (see Section X). In keeping with the results obtained from the scattering and field curvature studies of Sections VII and VIII, the overall length of each dipole antenna was less than 0.8 cm, i.e., less than 0.065 λ at 2450 MHz and less than 0.0244 λ at 915 MHz. The detector diodes employed were point contact silicon detector diodes type MA41512. The other detector circuit components comprised of two 1 KΩ 1/16 watt miniature resistors and one 500 pf microwave chip capacitor.

Performance tests on the prototype probe were in general satisfactory. The use of a very small high impedance antenna with a low impedance dc feed line produced excellent low noise and back-scatter performance. The noise level indicated on the VTVM in the absence of a signal was less than 10 microvolts and could not be readily distinguished from the voltmeter noise at this level. No significant back-scatter could be detected when the probe was used close to a radiating aperture providing the probe body was correctly aligned (see Section VII.C). Figure 21 shows the input/output characteristic of the probe over a 40 dB dynamic range. Because of the low noise figure realized

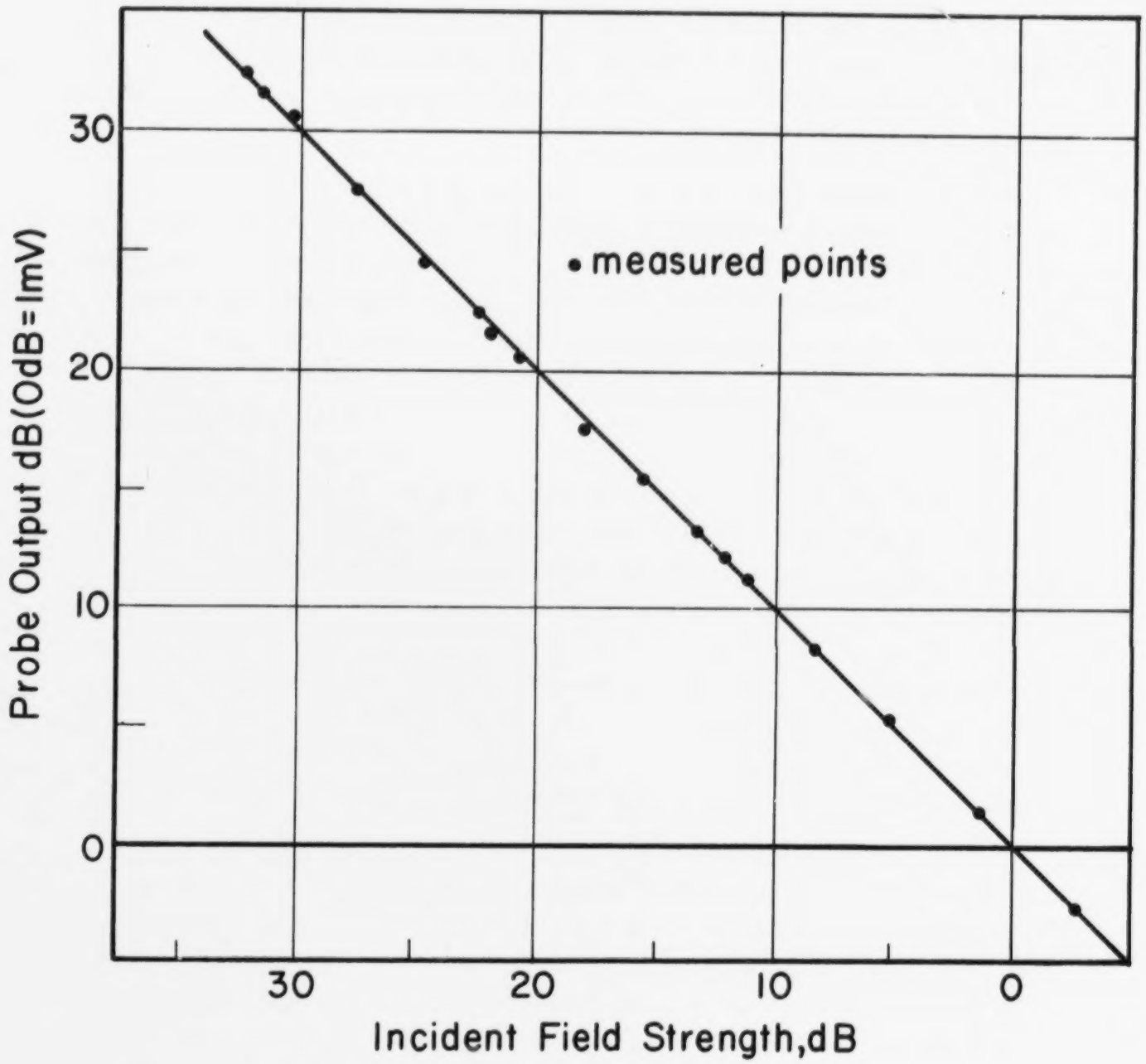

Figure 21. The prototype probe dynamic range measurements.

it is possible to use the probe over a maximum dynamic range of 47 dB with an accuracy of better than 0.5 dB over 44 dB of this range and better than 1.0 dB over the complete range.

Two practical problems were encountered in performance tests on the prototype probe. The silicon point contact diodes employed in the probe head were not well matched over the complete dynamic range. As a result the elipticity ratio (see Section X) of the probe antenna varies from 0.2 dB on the "LOW" range to a maximum elipticity of 1.5 dB. Due to delays encountered in the supply of both the matched silicon diodes and the microwave chip capacitors this could not be rectified in the time available. However, the prototype probe illustrates the techniques involved and the difficulty is not a fundamental one. The dynamic range obtainable with the prototype probe has been shown to be in excess of 40 dB, however, relative to the specified minimum field strength the probe dynamic range is from +33 dB to -14 dB. To provide a greater dynamic range above the minimum field strength it is only necessary to reduce the probe antenna gain by the techniques described in Section X. In view of the component supply difficulties encountered it was not possible to do this within the time scale available.

Although time constant specifications were not included in this program some preliminary investigation indicates that the diode detector probe has considerable advantages over other types of detector. If required very short time constants can be achieved by suitable design. For example, the prototype probe, which has not been optimized in this direction has a capacitor charging time constant of the order of 1.0 microsecond and (on the 915 MHz "MID" range) a discharge time constant of the same order. A useful demonstration of this feature can be obtained by connecting the output of the control box to a Tectronix oscilloscope with a bandwidth limitation of 5 MHz. The probe can then be placed in a electric field modulated by a

suitable pulse waveform. For this demonstration the frequency selector switch should be at 915 MHz regardless of the RF frequency involved. A calibration correction of 1.11 times will apply if the RF frequency is 2450 MHz. When switched to the 2450 MHz position the 1.0 Megaohm potentiometer used to correct the calibration factor will increase the time constant. This effect can be easily designed out if a fast response is specified for the probe.

XII. CONCLUSIONS AND SUGGESTIONS FOR FURTHER WORK

This report has described a short experimental study leading to the design, construction and calibration of a prototype near-field electromagnetic radiation probe. A basic probe configuration, employing a small dipole probe with a diode detector and filter circuit has been adopted and shown to have a number of advantages over alternative configurations.

The experimental study has been concerned with the sources of calibration errors arising from the use of small dipole antenna probes (calibrated in a free space environment) in close proximity to electromagnetic sources. The potential errors have been considered in two steps: the calibration errors involved in making measurements of electric field strength close to electromagnetic sources and the additional errors incurred in attempting to convert an accurate field strength measurement into a power density indication by means of a fixed calibration factor. The study has examined the effects of back-scatter by the dipole probe with regard to multiple coupling with the source and with respect to variation of the dipole impedance due to the close proximity of metallic objects. In addition, perturbation of the electric field due to the probe body and feed lines and the effects of curvature in the electric field lines close to a source have been briefly examined. The electromagnetic sources considered were the narrow slot in a groundplane and the thin current radiator.

The study has indicated that accurate measurements of electric field strength can be made very close to the electromagnetic sources considered, by suitable probe design. However, more severe limitations exist when it is desired to convert an accurate field strength measurement into a power density indication by means of a fixed calibration factor. No attempt has been made to determine a universal calibration correction for power density indications, in that it has been shown that such a correction will be dependent upon the particular source

configuration. However, worst case source distributions, with respect to this calibration error have been proposed for the "slot in groundplane" and "current radiator" sources, to provide maximum potential error curves relative to the probe-source spacing. These curves will at least be relevent to measurements close to sources of this type and may be valid for wider applications in that the two cases considered are basic TE and TM mode sources.

Practical guidelines from these results indicate that a far-field power density calibration on an accurate electric field strength probe will be less than 3 dB in error at probe to source spacings of greater than $\lambda/2\pi$, for practical source configurations of the type considered, providing the probe antenna is correctly aligned with the transverse field. For TM sources an incorrectly oriented probe can lead to apparent power density indications from a purely reactive field. In this case a probe to source spacing of greater than 2.2 $\lambda/2\pi$ is necessary to ensure that the peak value of the apparent power density is not greater than the real power density at the same point.

It is of interest to note that reactive fields will excite current flow in a load and from the viewpoint of radiation hazard such fields and their "apparent" power densities should not be neglected. If radiation hazard levels are expressed in terms of electric field strength directly, or in terms of "apparent" power density (which is merely an accurate measure of electric field strength converted to a power density via some fixed calibration factor) then the problems incurred in converting field strength measurements to real power flow could be largely circumvented.

Combining the results of this study with further work described in the text, a prototype near-field probe has been designed and constructed. For comparison with the near-field probes commercially available at the present time the final

design offers the following potential advantages.

1. Wide dynamic range (up to 47 dB).
2. Largely insensitive to ambient temperature variations.
3. Covers both frequency bands without change of component parts.
4. Small probe antenna (0.8 cm overall dipole length).
5. Negligible back-scatter.
6. Output independent of polarization of incident wave.
7. Short time constant for waveform studies.
8. Operates with any high impedance voltmeter or oscilloscope.
9. Output voltage directly proportional to apparent power density (or $|E|^2$).
10. Excellent sensitivity for low level work (0.0007 mW/cm^2 or lower).

The basic probe configuration described in this report is very flexible and can be readily adopted to provide an optimum performance for particular applications.

The work described in this report has been in no way exhaustive. In many respects the surface of the problem has hardly been scratched. In particular, there is a need for further work in the area of near-field measurements to establish whether the worst case power density calibration error curves for the "slot in groundplane" and "current radiator" sources can be applied in general to any source configuration. In connection with this study it is of great importanceto determine whether a measurement of electric field strength or "apparent" power density might have more merit as a standard than the present real power density (or power flow) with all its attendent calibration problems.

In the direction of near-field instrumentation several areas of interest remain outstanding. The design of a highly accurate electric field probe based on the experience obtained in the development of the prototype and tailored for specific application requirements would be of value. Such a probe might incorporate a very short time constant for waveform studies in addition to the dynamic range, sensitivity, polarization and multiple frequency specifications. The probe could also be adaptable for use in specific biological applications if required. Further work leading to improvements in the probe feed line problem is also required for applications where the source direction is either unknown or indeterminate. The use of a dielectric transmission line may have merit in this application.

If real power flow is to remain as the standard measurement in the near-field then the development of a near-field probe which overcomes the power density calibration error by measuring both the electric and magnetic field components simultaneously is a necessary step. Use of a Hall effect device is one possible approach to this problem.

The suggestions here are only a few of the possible directions for further research in this area. In particular, an extension of the basic studies into the problems associated with near-field measurements is of vital importance if any confidence is to be placed in present near-field standards and the extensive biological work now in progress.

REFERENCES

1. Jorden, E.C., Balmain, K.G., "Electromagnetic Waves and Radiating Systems", 2nd. ed., Prentice-Hall Inc. New Jersey, 1968.

2. Wolff, E.A., "Antenna Analysis", John Wiley and Sons, Inc., New York, 1966.

3. Slater, J. C., "Microwave Transmission" Dover Publications, 1969.

4. Midgely, D., "A Theory of Receiving Aerials Applied to the Re-Radiation of an Electromagnetic Horn", IEE Proc., 108B, 1961, pp. 645-649.

5. Kraus, J.D., "Antennas", McGraw-Hill Book Co., New York, 1950.

6. Montgomery, C.G., "Techniques of Microwave Measurements", Vol. 11 of the MIT Rad Lab Series, McGraw-Hill Book Co., 1947, p. 108.

7. Torrey, H.C. and Whitmer, C.A., "Crystal Rectifiers", Vol. 15 MIT Rad LAB Series, McGraw-Hill Book Co., 1948, p. 3.

8. Montgomery, C.G., "Techniques of Microwave Measurements", Vol. 11 of the MIT RAD LAB Series, McGraw-Hill Book Co., 1947, p. 189.

9. Vogler, L.E., Noble, J.L., "Curves of Input Impedance Change Due to Ground for Dipole Antennas", National Bureau of Standards, Monograph 72, Issued Jan. 31, 1964, Boulder, Colorado.

10. Sunde, D.E., "Earth Conduction Effects in Transmission Systems", Dover Publications, 1968.

11. "High Frequency and Microwave Field Strength Precision Measurements Seminar", National Bureau of Standards Report, Boulder, Colorado, March 1966.